Thorium(IV) and Uranium(IV) *trans*-calix[2]benzene[2]pyrrolide Alkyl and Alkynyl Complexes: Synthesis, Reactivity and Electronic Structure

Markéta Suvova,[†] Kieran T. P. O'Brien,[‡] Joy H. Farnaby,[†§] Jason B. Love,[†] Nikolas Kaltsoyannis,*[‡] and Polly L. Arnold *[†]

[†] EaStCHEM School of Chemistry, University of Edinburgh, The King's Buildings, Edinburgh, EH9 3FJ, United Kingdom

[‡] School of Chemistry, The University of Manchester, Oxford Road, Manchester M13 9PL, United Kingdom

Supporting Information Placeholder

ABSTRACT: The first thorium(IV) and uranium(IV) hydrocarbyl complexes of a *trans*-calix[2]benzene[2]pyrrolide macrocycle can use ligand non-innocence to enable multiple C-H bond activation reactions at the metal. Both alkyl and alkynyl complexes supported by the (L) dianion and (L^{-2H}) tetraanion are reported. The Th^{IV} and U^{IV} mono-alkyl –ate complexes [M(L^{-2H})An(R)] (M = K for R = CH_2Ph, M = Li for R = Me, CH_2SiMe_3), in which the ligand aryl groups are metallated, add the C-H bonds of terminal alkynes across the metal and ligand, forming the An^{IV}-alkynyl complexes [(L)An(C≡CR')$_2$] (R' = $SiMe_3$, Si^iPr_3). This ligand reprotonation from $(L^{-2H})^{4-}$ to $(L)^{2-}$ is accompanied by a change in coordination mode of the ligand from $\eta^5{:}\eta^5$ to $\eta^5{:}\eta^1{:}\eta^5{:}\eta^1$. Alternatively, the original alkyl group can be retained if the ligand is reprotonated using [Et_3NH][BPh_4], affording the Th^{IV} cations [(L)Th(R)][BPh_4] (R = CH_2Ph, $N(SiMe_3)_2$). Again, ligand rearrangement to the $\kappa^1{:}\eta^6{:}\kappa^1{:}\eta^6$ coordination mode occurs. These complexes provide rare examples of bis(arene) actinide sandwich geometry. The two η^1-alkynides in [(L)Th(C≡CSiMe$_3$)$_2$] rearrange upon coordination of [Ni^0], forming [(L)Th(C≡CSiMe$_3$)$_2$·Ni(PR''$_3$)] (R'' = phenyl, cyclohexyl) – featuring the shortest yet reported distance between Th and Ni, and giving unprecedented insight into the changes in macrocyclic ligand coordination between $\kappa^1{:}\eta^6{:}\kappa^1{:}\eta^6$ and $\eta^5{:}\eta^5$ coordination modes. A computational study of this conformational change demonstrates the $\eta^5{:}\eta^5$ coordination mode to be the more stable in the Th/Ni bimetallics (and hypothetical Pt analogues), an observation rationalised by detailed analysis of the Kohn-Sham orbital structure of the $\kappa^1{:}\eta^6{:}\kappa^1{:}\eta^6$ and $\eta^5{:}\eta^5$ conformers. Although remarkably inert to even high-pressures of CO_2 at room temperature, the bis(alkynyl) complexes [(L)An(C≡CSiMe$_3$)$_2$] completely cleave one CO bond of CO_2 when heated under a 1 bar pressure, resulting in the formation, and elimination from the metal, of a new, CO-inserted, bicyclic, carbonylated macrocycle with complete control over the C-C and C-N bond forming reactions.

INTRODUCTION

Organometallic f-block alkyl complexes show exciting reactivity in C–H bond activation.[1] Examples include the uranium(III) mediated formation of both "tuck-in" and "tuck-over" products from intra- and inter-molecular pentamethylcyclopentadienyl (Cp*) C–H bond activation,[2-4] C–H activation of typically inert carbocycles induced by steric crowding,[5] or the addition of C-H bonds across f-block metal imido and nitrido bonds.[6-10]

This is important because C–H bond activation is a key step in the synthesis of a range of desirable organic products. In spite of the many successful examples of d-block hydrocarbon C-H bond activation, there are no reports of an economically viable, homogeneous, catalysed process.[11-12]

Thorium(IV) and uranium(IV) coordination complexes have been studied for the last 60 years,[13] showing not only some interesting C–H bond reactivity, for example the intramolecular C–H bond activation of the methyl group on bis(permethylcyclopentadienyl) (Cp*) by the transient terminal uranium(IV) nitride complex [$Cp^*_2U(N)(N(SiMe_3)_2)$],[14] but also some interesting differences between Th^{IV} and U^{IV} complexes that would not have been predicted *a priori*.[15] For example, the activation of sp^3 hybridised bonds by [$(Cp^*)_2Th(R)_2$] (R = Me, CH_2Ph) in 2,6-lutidine *N*-oxide, does not take place with the uranium analogue of this system.[16]

The vast majority of studies of actinide alkyl reactivity have been carried out on complexes supported by the *bis*-Cp* ligand system, with the general formula [$(Cp^*)_2AnR_2$]

(R = hydrocarbyl).[16-28] We recently reported the synthesis of new *trans*-calix[2]benzene[2]pyrrolide $(L)^{2-}$ complexes of U^{III}, Th^{IV} (**A** in Scheme 1) and U^{IV} (**B**).[29] The bis(pyrrolide)-containing macrocycle $(L)^{2-}$ commonly binds to the An^{IV} cations through η^5-pyridyl ligation, affording complexes reminiscent of the metallocene dialkyls $[(Cp^*)_2An(R)_2]$.

However, L has a greater flexibility and range of binding modes than that available to the $[(Cp^*)_2AnR_2]$ complexes, including the facile conversion between η^5- and κ^1-pyrrolide coordination, the ability to incorporate cations in the cavity between the arene rings of the macrocycle (bis(arene) pocket), and the ability to bind the arene in the macrocycle as an η^1-aryl group, through further ligand deprotonation. Accordingly, we have studied the alkylation chemistry of these An^{IV} complexes **A** and **B**, and report herein the synthesis and reactivity of the first thorium(IV) and uranium(IV) alkyl and alkynyl complexes supported by the non-innocent macrocyclic $(L)^{2-}$, including rare examples of bis(arene) sandwich coordination of a thorium ion, the first structurally characterised thorium alkynyl complexes, and an unusual reversibility of the thorium-aryl – thorium-arene bonding with a ligand that enables new hydrocarbon functional group interconversion at the actinide centre. Furthermore, the isolation of new bimetallic complexes of the form $[(L)Th(C{\equiv}CSiMe_3)_2{\cdot}Ni(PR''_3)]$ (R'' = phenyl, cyclohexyl) gives insight into unprecedented changes in macrocyclic ligand coordination between $\kappa^1{:}\eta^6{:}\kappa^1{:}\eta^6$ and $\eta^5{:}\eta^5$ coordination modes. The latter mode is found by DFT calculations to be significantly more stable than the former in these bimetallic complexes, and analysis of the Kohn-Sham orbital structure provides a pleasing rationalisation of this energetic preference.

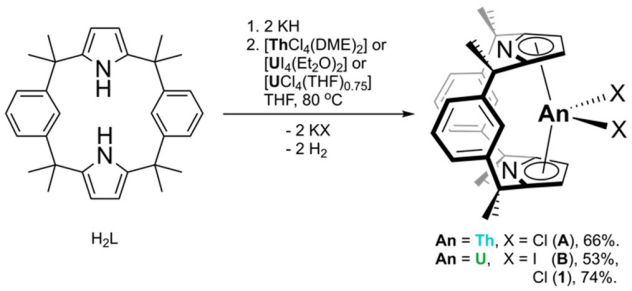

Scheme 1. Syntheses of $[(L)ThCl_2]$ (**A**), $[(L)UI_2]$ (**B**) and $[(L)UCl_2]$ (**1**).

RESULTS AND DISCUSSION

Synthesis of $[M(L^{-2H})An(R)]$. The syntheses of the chlorido-thorium complexes **A** and iodo-uranium complex **B** were reported previously, using a salt-metathesis strategy (Scheme 1).[29] Using an analogous procedure, orange crystalline $[(L)UCl_2]$ (**1**) (see SI Fig. S1 for molecular structure) is also accessible from $UCl_4(thf)_{0.75}$ and potassium salt $K_2(L)$ in 74% yield after work-up (see SI for solid-state structure). Characterisation of **1** by NMR spectroscopy and X-ray crystallography shows that **1** is isomorphous with **A** and **B**. With the aim of synthesising Th^{IV} and U^{IV} alkyl complexes, **A** and **1** were treated with three equivalents of MR (M = K for R = CH_2Ph, M = Li for R = Me, CH_2SiMe_3) in THF or toluene at ambient temperature over 18 hours (Scheme 2). Following work-up to remove MX and HR, the product $[M(L^{-2H})An(R)]$ was isolated arising from double aryl metallation to form the tetradentate $(L^{-2H})^{4-}$ ligand, and coordination of a single alkyl ligand, with the alkali-metal counter-cation residing in the bis(arene) pocket. It is important to note the addition of two equivalents of MR to **A** or **1** results in analogous reactivity to that described in Scheme 2 with unreacted **A** or **1** remaining.

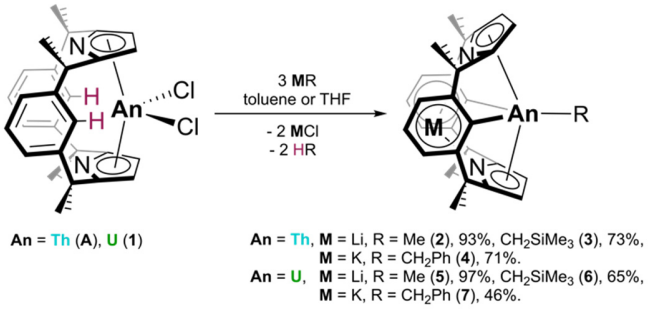

Scheme 2. Syntheses of $[M(L^{-2H})Th(R)]$ (R = Me (**2**), CH_2SiMe_3 (**3**), CH_2Ph (**4**) and $[M(L^{-2H})U(R)]$ (R = Me (**5**), CH_2SiMe_3 (**6**), CH_2Ph (**7**)).

The new complexes are isolated as yellow solids (R = Me (**2**) in 93% yield, CH_2SiMe_3 (**3**) in 73% yield, CH_2Ph (**4**) in 71% yield), and $[M(L^{-2H})U(R)]$ as dark orange solids (R = Me (**5**) in 97% yield, CH_2SiMe_3 (**6**) in 65% yield, CH_2Ph (**7**) in 46% yield). To our knowledge, complexes **2-7** are the first pyrrolic-macrocycle supported alkyl complexes of the actinides.

The ^1H NMR spectra of **2-7** show that the macrocyclic ligand in the new complexes retains the C_{2v} symmetry observed for **A** and **B**, where the methyl groups on the *endo* and *exo* faces of the macrocycle are represented by two singlets of equal integration. The ligand aryl deprotonation is characterised by the disappearance of the *ipso*-proton resonances in the ^1H NMR spectra of **2-7** and the dramatic increase in the *ipso*-carbon chemical shift in the $^{13}C\{^1H\}$ NMR spectra from 121.6 ppm in **A** to 217.6, 213.6 and 215.8 ppm in **2**, **3** and **4** respectively. In complexes **5-7**, the resonances are paramagnetically shifted and broadened due the U^{IV} f^2 ion. Single crystals suitable for X-ray diffraction studies were grown by vapour diffusion of hexane into saturated THF solutions of **2**, **3**, **4** and **6** at ambient temperature.

The molecular structures of **2** (Figure 1) and **4·THF** (Figure 2) display the tetradentate $\eta^5{:}\eta^1{:}\eta^5{:}\eta^1$ $(L^{-2H})^{4-}$ binding mode analogous to that in the Th^{IV} amido complex, $[K(L^{-2H})Th(N(SiMe_3)_2)]$ (**C**), previously reported by us.[29] In **2**, the lithium counter-cation occupies the cavity between the arene rings of the macrocycle. This motif is similar to that of **4·THF**, where the potassium counter-ion is additionally coordinated to a THF molecule and the benzyl group of the adjacent complex. Although complexes **3** and **6** are synthesised using the procedure described in Scheme 2, X-ray quality crystals could not be obtained. Subsequent addition of one equivalent of LiCl to **3** and **6** facilitates salt-bridged dimerization and the growth of X-ray quality crystals of **3·LiCl** and **6·LiCl·THF** (see SI Fig. S2 and S3 for molecular structures).

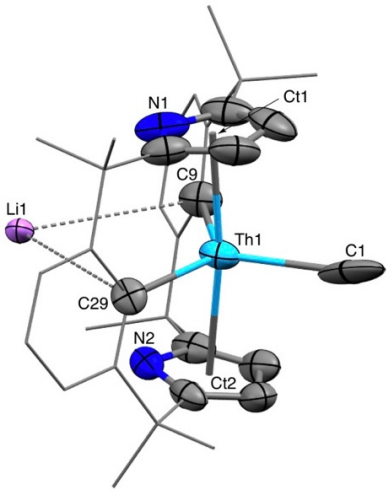

Figure 1. Solid state structure of **2** (thermal ellipsoids set at 50% probability level). Hydrogen atoms are omitted for clarity. Selected bond lengths (Å) and angles (°) for **2**: $[Th1–Ct]_{avg}$ 2.55, Th1–C1 2.65(2), Th1–C9 2.603(13), Th1–C29 2.603(11), Ct–Th1–Ct 172.26, C9-Th1-C29 129.9(4).

The Ct1–An–Ct2 (Ct = centroid) in the molecular structures of **2**, **3·LiCl**, **4·THF** and **6·LiCl·THF** are 172.26°, 168.48°, 170.16° and 172.03°, respectively; this is larger than that observed for **A** (163.60°) and **1** (164.97°). The C9–An–C29 angles are altered from **A** (120.50°) and **1** (120.88°) to 129.9(4)°, 120.95(14)°, 115.4(6)° and 124.33(12)° in **2**, **3·LiCl**, **4·THF** and **6·LiCl·THF**, respectively. These data indicate the flexibility of the macrocyclic ligand framework given varying sizes of both M^+ and the R substituents. The Th1–C1 bond length in **2** is 2.65(2) Å, which is longer than that reported for Th^{IV}–Me bond average (2.53 Å) in metallocene-like complexes.[16, 18, 27, 30-36] The An–C1 bond lengths in **3·LiCl**, average 2.532(5) Å, **4·THF**, average 2.58(2) Å, and **6·LiCl·THF**, 2.489(4) Å, are similar to literature values.[4, 37-47]

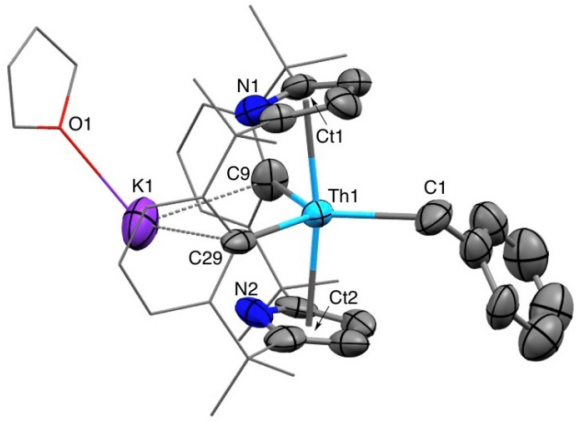

Figure 2. Solid state structure of **4·THF** (thermal ellipsoids set at 50% probability level). Hydrogen atoms are omitted for clarity. Selected bond lengths (Å) and angles (°) for **4·THF**: $[Th1–Ct]_{avg}$ 2.53, Th1–C1 2.58(2), Th1–C9 2.55(3), Th1–C29 2.59(2), $[Ct–Th1–Ct]_{avg}$ 170.16, C9–Th1–C29 115.4(6).

Selective Ligand Reprotonation of [M(L^{-2H})An(R)]. The An–aryl bonds in the [M(L^{-2H})An(R)] complexes **2-7** provide a useful route to new hydrocarbon C–H bond reactivity pathways, exemplified by the reaction with terminal alkynes (Scheme 3). Two equivalents of HC≡CR' (R' = $SiMe_3$, Si^iPr_3) were added to a suspension of **2** or **5** in hexanes at room temperature and stirred for 16 hours. Following work-up to remove the unusual by-product LiMe, the reprotonated $(L)^{2-}$ complexes were isolated as pale yellow solids [(L)Th(C≡CSiMe_3)$_2$] (**8**) and [(L)Th(C≡CSi^{i}Pr$_3$)$_2$] (**9**) or red solids [(L)U(C≡CSiMe_3)$_2$] (**10**) and [(L)U(C≡CSi^{i}Pr$_3$)$_2$] (**11**) in 44%, 54%, 50% and 50% yield, respectively. The addition of an excess of HC≡CR' does not alter the outcomes or yields of these reactions.

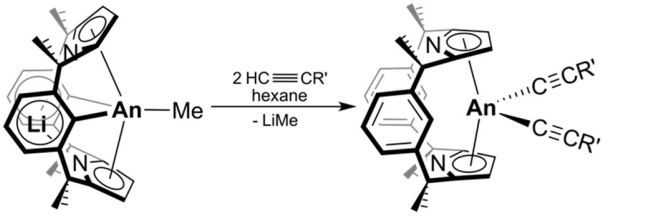

Scheme 3. Syntheses of [(L)Th(C≡CSiMe_3)$_2$] (**8**), [(L)Th(C≡CSi^{i}Pr$_3$)$_2$] (**9**), [(L)U(C≡CSiMe_3)$_2$] (**10**) and [(L)U(C≡CSi^{i}Pr$_3$)$_2$] (**11**).

The C_{2v} symmetry in **8-11** is retained. The aryl *ipso*-proton resonances are observed in the ^{1}H NMR spectra and in the $^{13}C\{^1H\}$ NMR spectra and are shifted from 217.6 ppm in **2** to 123.9 and 123.7 ppm in **8** and **9**, respectively. Pale yellow single crystals of **8** and **9** were isolated from saturated benzene solutions. The synthesis of **8** and **9** was also attempted from **3**, however the reactive by-product $LiCH_2SiMe_3$ has a very similar solubility to **8** and **9**, preventing the isolation of pure material.

The molecular structures of **8**, **9** and **11** (Figure 3 and SI Fig. S4 and S5 for **9**, and **11**) display bidentate η^5:η^5 binding, analogous to that of **A**. The Ct1–An–Ct2 angles in **8**, **9** and **11** are 169.49°, 169.43° and 170.44°, respectively; larger than in **A** (163.60°) and **1** (164.97°). This subtle change in geometry is likely to be the result of the smaller covalent radius of carbon compared to that of chloride.[48]

Although reactivity involving Th^{IV} alkynyl complexes has been invoked,[49-51] to the best of our knowledge **8** and **9** are the first crystallographically characterised thorium alkynyl complexes. A few uranium(IV) alkynyl complexes have been reported to date;[18, 52-57] metallocene-like systems reported in the literature display similar U^{IV}–alkynyl bond lengths to the U1–C1/C3 average distance in **11**, 2.408(9) Å.

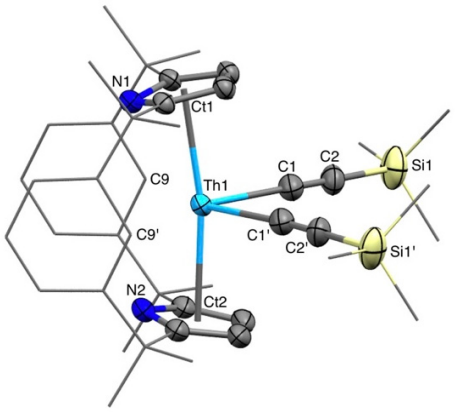

Figure 3. Solid state structure of **8** (thermal ellipsoids set at 50% probability level). Hydrogen atoms are omitted for clarity. Selected bond lengths (Å) and angles (°) for **8**: $[Th1–Ct]_{avg}$ 2.532, Th1–C1 2.479(4), C1–C2 1.220(5), Ct–Th1–Ct 169.49, C9–Th1–C9' 128.10; **9**: $[Th1–Ct]_{avg}$ 2.54, Th1–C1 2.482(3), Th1–C3 2.471(3), C1–C2 1.219(4), C3–C4 1.207(4), Ct–Th1–Ct 168.36, C9–Th1–C29 124.15; **11**: $[U1–Ct]_{avg}$ 2.48, U1–C1 2.378(9), U1–C3 2.437(8), C1–C2 1.236(11), C3–C4 1.205(11), Ct–U1–Ct 170.44, C9–U1–C29 124.91.

Selective Ligand Reprotonation of [K(L^{-2H})Th(R)]. The C–H addition route described above forms the Th-alkynyl group and reprotonates the ligand aryl rings from $(L^{-2H})^{4-}$ to $(L)^{2-}$. Alternatively, the R group can be retained, and the cationic complex formed if the weak acid $[Et_3NH][BPh_4]$ (pKa of 9 in DMSO)[58] is used to reprotonate the ligand aryl groups: two equivalents of $[Et_3NH][BPh_4]$ were added to a solution of **4** in THF and the suspension stirred at ambient temperature for two hours (Scheme 4). After work-up to remove the volatile Et_3N and insoluble $K[BPh_4]$ by-products, $[(L)Th(CH_2Ph)][BPh_4]$ (**12**) can be isolated as an off-white solid in 31% yield. The analogous amido complex $[(L)Th(N(SiMe_3)_2)][BPh_4]$ (**13**) is also accessed in this manner, in a 68% yield, from $[K(L^{-2H})Th(N(SiMe_3)_2)]$ (**C**), a complex previously reported by us.[29] The addition of an excess of $[Et_3NH][BPh_4]$ to **4** or **C** does not affect the yield of products **12** or **13**.

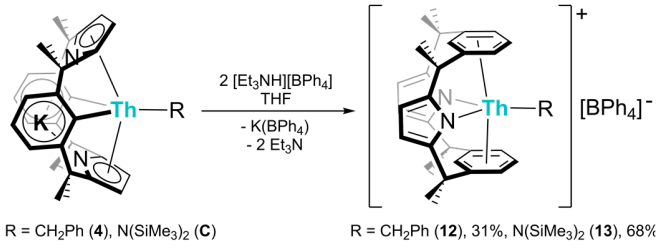

Scheme 4. Syntheses of $[(L)Th(CH_2Ph)][BPh_4]$ (**12**) and $[(L)Th(N(SiMe_3)_2)][BPh_4]$ (**13**).

X-ray structural characterisation of **13** (Figure 4) indicates that the ancillary ligand $(L)^{2-}$ adopts an $\eta^6{:}\kappa^1{:}\eta^6{:}\kappa^1$ coordination to the Th^{IV} cation thus forming a bis(arene) sandwich complex. Thorium arene interactions are rare, with only a few examples reported in the literature.[39, 59-62] This binding mode of $(L)^{2-}$ has previously been observed for U^{III} and Np^{III} complexes of the form [(L)AnX] (X = I, BH_4, $N(SiMe_3)_2$, O-2,6-^{t}Bu$_2$-C_6H_3 for U^{III} and X = Cl for Np^{III}) and $[(L)Np_2Cl_4(THF)_3]$ but not for complexes of An^{IV}.[29, 63-65] Multinuclear NMR spectroscopic analysis suggests that **12** and **13** are analogues, however X-ray quality single crystals of **12** could not be obtained and the coordination mode of $(L)^{2-}$ in **12** could not be determined.

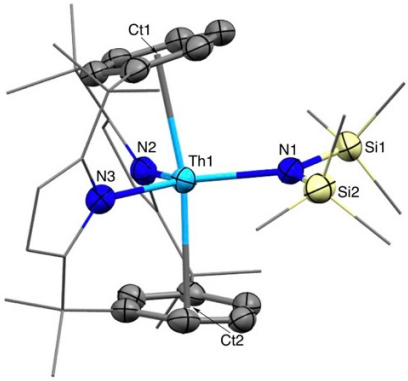

Figure 4. Solid state structure of **13** (thermal ellipsoids set at 50 % probability level). The $[BPh_4]^-$ counterion and hydrogen atoms are omitted for clarity. Selected bond lengths (Å) and angles (°) for **13**: Th1–$[aryl]_{Ct(avg)}$ 2.690, Th1–N1 2.469(5), Th1–N2 2.483(5), Th1–N3 2.276(5), $[aryl]_{Ct1}$–Th1–$[aryl]_{Ct2}$ 169.41, N1–Th1–N2 115.47(16).

The Th1–$[aryl]_{Ct(avg)}$ distance in **13** (2.690 Å) is similar to that in a polydentate pyrrolide-containing thorium(IV) arene complex $[Li(DME)_3][\eta^6\text{-}\{1,3\text{-}[(2\text{-}C_4H_3N)(CH_3)_2C]_2C_6H_4\}ThCl_3]$ (2.701(8) Å).[60] Examples of interactions between Th^{IV} and η^6-coordinated arene molecules in the literature show bond lengths between 2.815(3) Å and 4.05(1) Å, which are longer than the Th1-$[aryl]_{Ct(avg)}$ bond distance in **13**.[39, 59, 62]

A decrease of the Th1–N3 bond from 2.375(12) Å in **C**,[29] to 2.276(5) Å in **13** is observed, a decrease which is likely to result from the cationic nature of **13**. The Th1–N1 distance in **13** is also shorter than other Th^{IV}–$N(SiMe_3)_2$ literature bonds.[61, 66-69]

The U^{III} complexes [(L)UI] and [(L)UI(THF)] have $[aryl]_{Ct1}$–U–$[aryl]_{Ct2}$ angles of 173.55° and 171.61°, respectively,[29] and the samarium(III) [(L)SmCl] complex has a $[aryl]_{Ct1}$–Sm–$[aryl]_{Ct2}$ angle of 179°.[70] The base-free U^{III} and Sm^{III} complexes display larger angles, (*i.e.* closer to idealised bis-arene binding) whilst the angle in [(L)UI(THF)] is decreased, most likely as a result of steric repulsion caused by the THF molecule. This can be used to explain the notably smaller $[aryl]_{Ct1}$–Th1–$[aryl]_{Ct2}$ angle in **13** (169.41°) that is likely to be the result of steric repulsion caused by the bulky $N(SiMe_3)_2$ ligand. Although the U^{III} analogue of **13**, $[(L)U(N(SiMe_3)_2)]$,[63] displays a larger $[aryl]_{Ct1}$–U–$[aryl]_{Ct2}$ angle (176.05°) than that in **13**, the bulky $N(SiMe_3)_2$ ligand is further away from the metal centre in the U^{III} complex: the U1–N3 bond (2.364(3) Å) is longer than the Th1–N3 bond in **13** (2.276(5) Å).

Discussion of the Reversible Aryl Metallation. Evans showed that the addition of two equivalents of HC≡CPh to $[(Cp^*)_2U(Me)_2]$ results in the synthesis of $[(Cp^*)_2U(C{\equiv}CPh)_2]$ and methane elimination.[53] A survey of

metallocene-like Th^{IV} and U^{IV} complexes shows that the bond dissociation energies of An–alkyl bonds are generally lower than those of An–aryl bonds.[25, 71-73] Interestingly, Marks showed that the U–alkynyl bond dissociation enthalpy in the complex $[Cp''_3U(C{\equiv}CPh)]$ (Cp'' = η^5-$C_5H_4SiMe_3$) is nearly twice that of U–Me in the analogous methyl complex $[Cp''_3U(Me)]$, however Marks did not make a direct comparison with U–aryl bond enthalpies.[73] We have shown that An–arene bonds in complexes **2** or **5** can be reprotonated to give $(L)^{2-}$ by the alkynes $HC{\equiv}CR'$ (R' = $SiMe_3$, Si^iPr_3) (pKa of acetylenes in DMSO: ~28)[74] or the weak acid $[Et_3NH][BPh_4]$ (pKa in DMSO: 9).[58] These findings suggest that the formation of **8-11** is in part driven by the formation of the stronger An–alkynyl bond. The synthesis of **12-13** is likely driven by the acidity of $[Et_3NH][BPh_4]$.

Reactivity of 2-13 Towards Small Molecules.

Actinide complexes have been shown to effect unique small molecule transformations relative to d-block metals.[75] Complexes **2-7** contain three actinide-carbon σ-bonds. The additions of small molecules such as CO, CO_2 or ^{t}BuNC with the aim of An–C bond insertion have been carried out to understand if selective insertion processes might be useful for ligand functionalisation prior to the selective reprotonation; the reactions are summarised in Scheme 5.

$[M(L^{-2H})\mathbf{An}(R)]$ (**2-8**) $\xrightarrow{CO\ /\ CO_2\ /\ ^t BuNC}$ mixtures of products

$[(L)\mathbf{Th}(R)][BPh_4]$ (**13-14**) $\xrightarrow{CO\ /\ CO_2\ /\ ^t BuNC}$ mixtures of products

$[(L)\mathbf{An}(C{\equiv}CSiR_3)_2]$ (**8-11**) $\xrightarrow{2\ bar\ CO\ /\ 10\ bar\ CO_2}$ no reaction

Scheme 5. Reactions to target the insertion of small, unsaturated substrates into An-C bonds.

Addition of CO or CO_2 to complexes **12** and **13** also results in indistinguishable mixtures of products. The reactivity of the An–C alkynyl bonds in complexes **8-11** was also investigated. These bonds are inert to CO_2 insertion at 10 bar and CO insertion and reaction with H_2 at 2 bar. The stability of uranium(IV)-alkynyl bonds towards CO_2 insertion in metallocene-like complexes has previously been reported, where pressures of 5.5 bar were required to insert CO_2 into an An-C bond.[55] It was found here, however, that heating either **8** or **9** in C_6D_6 under 1 bar of CO_2 results in CO_2 cleavage through *trans*-calix[2]benzene[2]pyrrolide ligand functionalisation and elimination from the metal, the loss of one oxo atom, presumably to the Th centre (Scheme 6) resulting in the formation of a new, CO-inserted, bicyclic calix-pyrrole $Me_2C(m\text{-}C_6H_4)(HNC_4H_2)(CMe_2)_2(o\text{-}CO\text{-}m\text{-}C_6H_4)(NC_4H_2)CMe_2$, LCO (**14**), in 70% crystalline yield (see SI Fig. S6 for X-ray structure of **14**). It is proposed that transient Th^{IV}–*oxo* complexes form as by-products that rapidly decompose yielding white insoluble solids. These Th^{IV} by-products could not be conclusively characterised; they have been drawn as Th^{IV}-mono-*oxo* for simplicity, however it is likely that *oxo*-bridged dimers or clusters form instead.

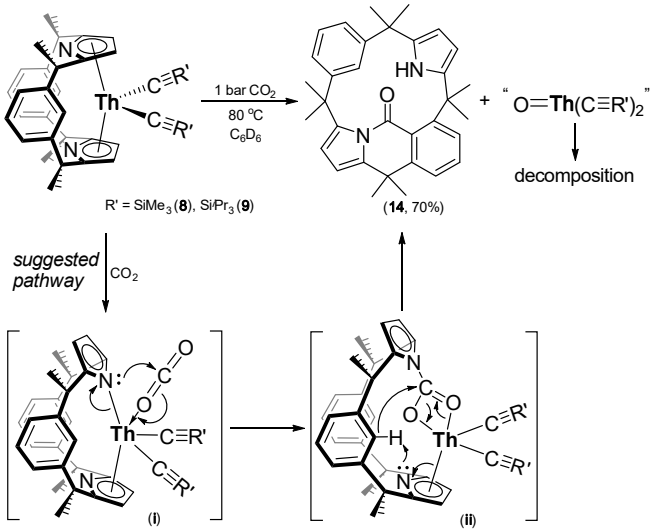

Scheme 6. Proposed reaction path of ancillary ligand functionalisation and abstraction from the thorium-metal centres of complexes **8** or **9** to form LCO, **14**.

Although the detailed mechanism of the formation of **14** has not been investigated, in the first step, shown in Scheme 6, CO_2 coordination to the metal centre is proposed, shown as intermediate **i**. The resulting steric crowding, in part due to the rigidity of the Th^{IV} alkynyl bonds, may then facilitate a ligand hapticipty shift to pyrrolide κ^1-N coordination. It has been established that CO_2 can insert into actinide-nitrogen bonds to form carbamate;[75-76] the suggested intermediate **ii** in Scheme 6. The non-innocence of this ligand system then allows for *ipso*-hydrogen migration to the pyrrolide, resulting in the formation of a demetallated derivative.

Nickel Coordination to 8 and Ligand Fluxionality. The inertness of the An–C alkynyl bonds in $[(L)Th(C{\equiv}CSiMe_3)_2]$ (**8**) and $[(L)Th(C{\equiv}CSi^iPr_3)_2]$ (**9**), led us to explore the reactivity of their π-systems. It has been established that group 10 transition metals readily coordinate unsaturated bonds.[77] Simple Group 4 $[(Cp)_2TM(C{\equiv}CSiMe_3)_2]$ (TM = Ti or Zr) bis-alkynyl complexes have shown nickel coordination to the C≡C triple bonds that is accompanied by TM^{IV}–C activation and ligand rearrangement of the alkynyl groups.[77] In order to establish whether this trend can be extended to Th^{IV}, $[(L)Th(C{\equiv}CSiMe_3)_2]$ (**8**) and $[(L)Th(C{\equiv}CSi^iPr_3)_2]$ (**9**), were treated with one equivalent of $Ni(COD)_2$ (COD = 1,5-cyclooctadiene) and PR''_3 (R'' = cyclohexyl, phenyl) (Scheme 7). Complex **8** reacts readily and after work-up to remove volatiles, no bound COD remains, according to NMR spectroscopy, and dark orange-red X-ray quality single crystals of the new complexes $[(L)Th(C{\equiv}CSiMe_3)_2{\cdot}Ni(PCy_3)]$ (**15a**) (Figure 5) or $[(L)Th(C{\equiv}CSiMe_3)_2{\cdot}Ni(PPh_3)]$ (**16a**) (see SI Fig. S7) were isolated from saturated hexane solutions in 7% and 18% crystalline, isolated yields, respectively. In the case of **9**, no reaction occurrs.

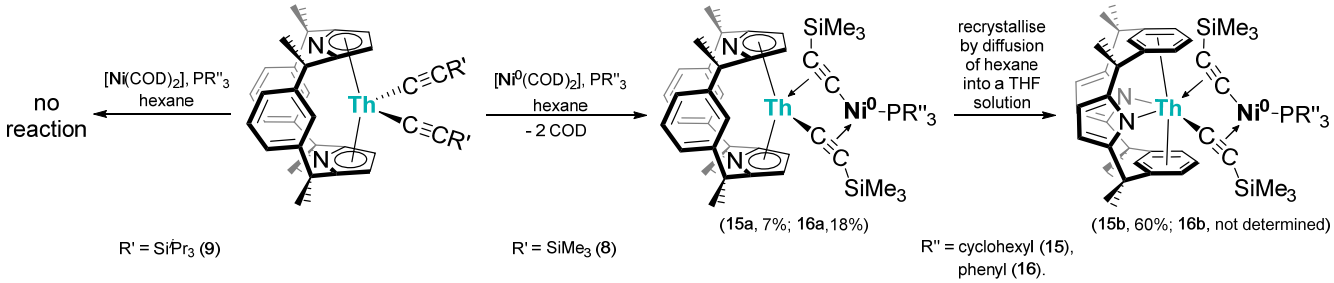

Scheme 7. Synthesis of [(L)Th(C≡CSiMe$_3$)$_2$·Ni(PCy$_3$)] (**15**) and [(L)Th(C≡CSiMe$_3$)$_2$·Ni(PPh$_3$)] (**16**) (Cy = cyclohexyl, COD = 1,5-cyclooctadiene) from **8**. The reaction does not proceed with **9**. Dissolution of the metallocene forms **15/16a** in THF enables the conversion to the bis(arene) form **15/16b.**

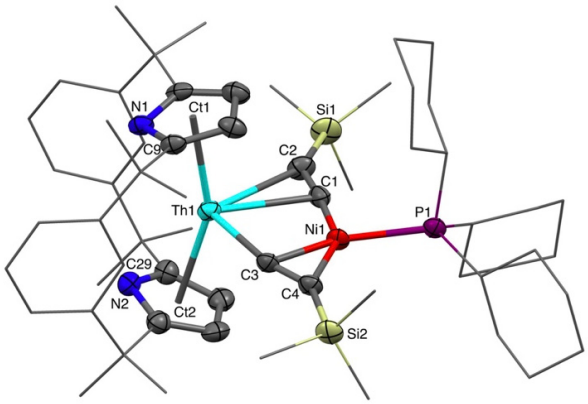

Figure 5. Solid state structure of **15a**, where single crystals were grown from a saturated solution of **15a** in hexane (thermal ellipsoids set at 50% probability level). Hydrogen atoms are omitted for clarity. Selected bond lengths (Å) and angles (°) for **15a**: [Th1–Ct]$_{avg}$ 2.557, Th1–C1 2.645(5), Th1–C2 2.937(6), Th1–C3 1.938(5), C1–C2 1.267(8), C3–C4 1.268(8), Ni1–C1 1.814(6), Ni1–C3 1.938(5), Ni1–C4 2.025(6), Ni1–P1 2.2053(16), Ct–Th1–Ct 155.61, C9–Th1–C29 113.86. **16a**: [[Th1–Ct]$_{avg}$ 2.563, Th1–C1 2.614(3), Th1–C3 2.423(3), C1–C2 1.246(4), C3–C4 1.272(4), Ni1–C1 1.829(3), Ni1–C3 1.932(3), Ni1–C4 2.015(3), Ni1–P1 2.1806(9), Ct1–Th1–Ct2 157.64, C9–Th1–C29 114.70.

As an alternative crystallisation method for **15**, hexane vapour was allowed to diffuse into a saturated THF solution of **15** yielding dark orange-red X-ray quality single crystals of [(L)Th(C≡CSiMe$_3$)$_2$(NiPCy$_3$)], **15b**, the molecular structure of which is shown in Figure 6. Surprisingly, the two methods of crystallisation of **15** yield two different binding modes for L, shown in Figs 6 and 7. When crystallised from hexane the (L)$^{2-}$ coordination mode is metallocene-like η^5:η^5 (**15a**); when crystallised from THF, the (L)$^{2-}$ coordination mode is η^6:κ^1:η^6:κ^1 (**15b**), like **13**. Although THF is found co-crystalised in the lattice of **15b**, computational analysis, discussed below, suggests that this is unlikely to affect ligand coordination.

A survey of the available literature indicates that only two heterobimetallic complexes featuring thorium and nickel adjacent to each other have been reported to date,[78-79] one of which is a Th^{IV} *bis*-Cp* nickel phosphido complex [(Cp*)$_2$Th(μ-PPh$_2$)$_2$Ni(CO)$_2$] (Th–Ni distance: 3.206(2) Å), where the authors suggest that an interaction between nickel and thorium exists.[79] The Th1–Ni1 distances in complexes **15a** (3.0559(7) Å), **15b** (3.053 Å) and **16** (3.068 Å) are notably shorter than those reported in the literature, and on average approximately 0.25 Å shorter than the sum of the covalent radii of nickel and thorium.[48]

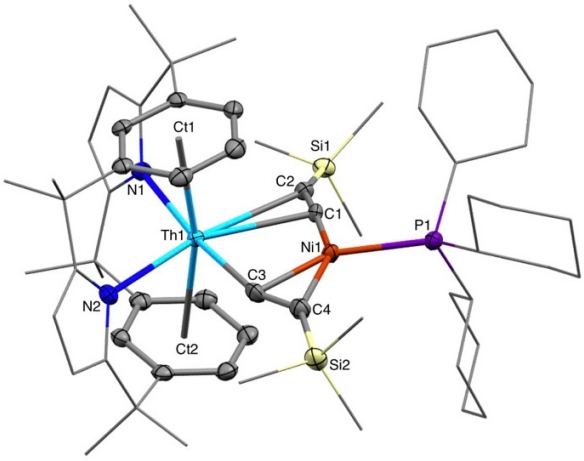

Figure 6. Solid state structure of **15b**, where single crystals were grown from the diffusion of hexane into a saturated solution of **15b** in THF (thermal ellipsoids set at 50% probability level). Hydrogen atoms are omitted for clarity. Selected bond lengths (Å) and angles (°) for **15b**: [Th1–Ct]$_{avg}$ 2.665, Th1–C1 2.653(3), Th1–C3 2.436(3), C1–C2 1.250(4), C3–C4 1.272(4), Th1–N1 2.604(2), Th1–N2 2.587(2), Ni1–C1 1.830(3), Ni1–C3 1.933(3), Ni1–C4 2.005(3), Ni1–P1 2.1999(8), Ct–Th1–Ct 166.55.

The solid-state structures of **15** and **16** show that the interaction with the Ni^0 centre is strong enough to reorganise the Th–C alkynyl groups from bis(η^1) to η^1 to one metal and η^2 to the other. This asymmetry was previously observed in the solid state structure of [(Cp)$_2$TM(C≡CSiMe$_3$)$_2$(NiPPh$_3$)] (TM = Ti, Zr).[77]

The solid state structures of **15a**, **15b** and **16** display a very slight increase in C≡C bond lengths compared to that of free HC≡CTMS (1.194(8) Å).[80] There is also a small lengthening of the triple bonds of the alkynyl ligands upon nickel binding in [(Cp)$_2$TM(C≡CSiMe$_3$)$_2$][NiPPh$_3$] (TM = Ti, Zr):

the IR stretching frequencies for these bonds are reported as 1780 and 1911 cm^{-1} for the titanium complex and 1771 and 1876 cm^{-1} for the zirconium complex.[77] These data differ from those for **16**, where the observed IR stretching frequencies are 2120 and 2071 cm^{-1}, indicating that only one C≡C stretch is notably shifted from the stretching frequency of the starting material **8** (2140 cm^{-1}) as a result of interactions with the Ni centre.

Complexes **15** and **16** are stable in the solid state for a number of weeks, although decompose in solution over several days. To further stabilise these complexes, attempts were made to increase the electron count around the nickel metal centre by using a bidentate four electron phosphine donor dppf (dppf = 1,1′-ferrocenediyl-bis(diphenylphosphine)). No reaction was observed between Ni(dppf)(COD) and **8,** Scheme 8, which may be caused by the bulk of the dppf ligand hindering the coordination of nickel to the alkynyl groups of **8.**

Reactions were carried out to target platinum analogues of **15** and **16**, **15'** and **16'**, using $Pt(nb)_3$ (nb = norbornene). However, the reaction of **8** with $Pt(nb)_3$ in donor solvents such as THF resulted in the formation of a mixture of products (Scheme 8). The addition of donor molecules designed to stabilise the putative product such as PCy_3 or PPh_3 did not yield a clean product. In a similar manner to Ni(dppf)(COD) no reaction with Pt(dppf)(nb) was observed.

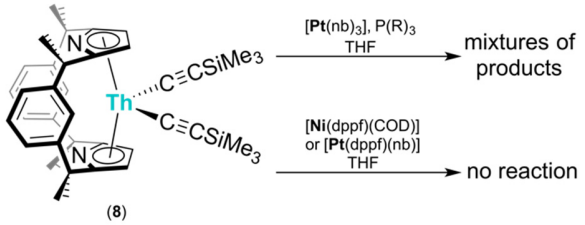

Scheme 8. Reactions to target **15'** and **16'**, platinum analogues of **15** and **16** (R = cyclohexyl, phenyl), $[(L)Th(C{\equiv}CSiMe_3)_2][Pt(dppf)]$ (dppf = 1,1′-Ferrocenediyl-bis(diphenylphosphine)) and $[(L)Th(C{\equiv}CSiMe_3)_2][Ni(dppf)]$.

Analysis of the flexibility of the macrocycle and alkynide binding.

A combination of variable temperature NMR spectroscopy and DFT computational studies was undertaken to interrogate the ligand flexibility and dynamic equilibria. Given the low isolated yields of **15**, and that computational analysis (discussed in detail below) shows that the Gibbs free energy difference between **15** and **16** is negligible (3.4 kJ·mol^{-1}), the variable temperature NMR spectral study of just **16** was undertaken.

The ^{1}H NMR spectra of **15** and **16** at 298 K correspond to a molecule with overall C_{2v} symmetry, indicating a symmetrical bis(alkynide) coordination on the NMR timescale in solution, but this is lowered to C_S as solutions are cooled to 190 K. Figure 7 shows the two halves of L in the **a** (metallocene) and **b** (bis arene) binding modes of **15**/**16** coloured blue and pink, that are inequivalent in the solid state structures, and at low temperatures in solution NMR spectroscopy, from the asymmetric alkynyl coordination.

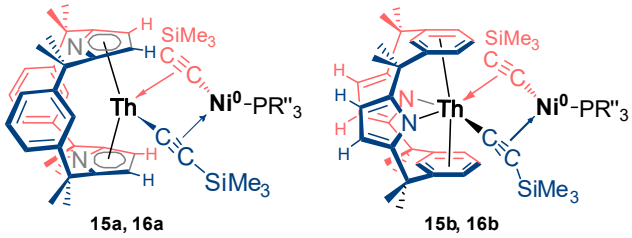

Figure 7. Plane of asymmetry introduced into **15** and **16** by alkynyl asymmetry in solid-state and low temperature solutions changes depending on coordination of $(L)^{2-}$. Hydrogens in one plane of symmetry are shown as blue and in the other plane as pink.

The flexibility of $(L)^{2-}$ also offers other dynamic equilibria processes that decoalesce sequentially as the temperature of either THF-d_8 or toluene-d_8 solutions of **16** are warmed from 190 K.

Careful inspection of the spectra at 193 K in THF-d_8 shows that the two pyrrolide-H resonances of the macrocycle are doublets. These are closest to the alkynide ligands in the conformation **a** (Figure 7 LHS), in which the pyrrolide-hydrogens on the same ring are no longer equivalent, suggesting a low-temperature solution-state state structure consistent with **16a**. The resonances of **16a**, gradually coalesce to a single, average chemical shift from 200-230 K. This suggests there is sufficient flexibility in the ligand binding that even when the alkynyl ligands are bound asymmetrically (on the NMR timescale) the macrocycle can flex such that an average C_{2v} can be maintained.

For comparison, the coalescence temperature for the process that renders the $SiMe_3$ groups equivalent in $[(Cp)_2Ti(C{\equiv}CSiMe_3)_2][NiPPh_3]$ is just above 190 K.[77] The ^{1}H NMR spectra of the dichloride **A** show no dynamic processes; spectra in THF-d_8 are the same at 193 K and 298 K.

Computational Analysis of 15, 16 and Pt analogues. In order to probe further the different conformations of the ancillary $(L)^{2-}$ ligand in complexes **15** and **16**, we turned to scalar relativistic, hybrid density functional theory. The hypothetical platinum analogues of these systems **15'** and **16'** have also been studied. The total SCF (E) and Gibbs (G) energies of the optimised geometries of the Th/Ni and Th/Pt systems are given in Tables S6 and S7 of the SI respectively, and the energy differences between the **a** (η^5:η^5) and **b** (η^6:κ^1:η^6:κ^1) forms of all four molecules are collected in Table 1. The negative numbers in Table 1 show that in all cases the **a** form is the more stable, with a greater preference for this conformation in the PPh_3 systems.

Table 1: ΔE and ΔG values (kJ mol^{-1}) between the a (η^5:η^5) and b (η^6:κ^1:η^6:κ^1) forms of 15, 16, 15' and 16'.

	ΔE	ΔG
15a – 15b	–24.8	–23.8
16a – 16b	–33.7	–27.2
15a' – 15b'	–25.6	–24.1
16a' – 16b'	–30.5	–27.3

By contrast to the data in Table 1, single point SCF energies of the $[(L)Th^{IV}]^{2+}$ fragment in geometry-optimised **15a** and **15b** show that this fragment is more stable, by 19.0 kJ mol^{-1}, in the $\eta^6{:}\kappa^1{:}\eta^6{:}\kappa^1$ conformation. The rest of **15** – *i.e.* the $[(CCSiMe_3)_2NiPCy_3]^{2-}$ fragment – has almost exactly the same energy in **15a** and **15b** (1.0 kJ mol^{-1} difference). Hence, the energetic preference for the **a** form of the full molecules must arise from differences in bonding between the $[(CCSiMe_3)_2NiPCy_3]^{2-}$ and $[(L)Th^{IV}]^{2+}$ fragments in the different L orientations. We assume that this is also the case for **16**. That the energy differences between the **a** and **b** forms of both **15** and **16** are very similar for their Pt analogues, suggests the group 10 transition metal has little impact here, but the larger preference for the **a** conformation for the PPh_3 systems hints at the R'' group having a greater role.

To establish the origin of the energetic preference for the $\eta^5{:}\eta^5$ bonding mode, we examined the valence Kohn-Sham molecular orbitals (MOs) of **15** and **16** to identify any with significant energy changes between the **a** and **b** conformations. Table S8 in the SI gives the energies of selected MOs for both compounds; the energies and isosurfaces for those of **15** are presented in Figure 8. The MOs labelled in red feature Ni-alkynyl interactions with an in-phase combination of Ni d and alkynyl π orbitals, the latter also being in phase with one another. For **15b**, there is only one such orbital (MO 266), which has only small contributions from the LTh fragment, whereas there are two MOs with this character in **15a** (MOs 267 and 255). This splitting of the Ni–alkynyl character in two **15a** MOs arises because in this conformation it is similar in energy to a Th-pyrrolide bonding MO, and this generates in phase and out of phase combinations (MOs 255 and 267, respectively). The former is significantly stabilised *vs* MO 266 of **15b**, while the latter is destabilised, albeit to a lesser extent.

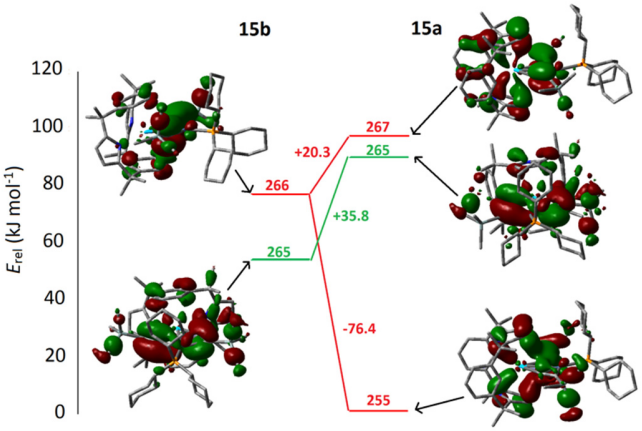

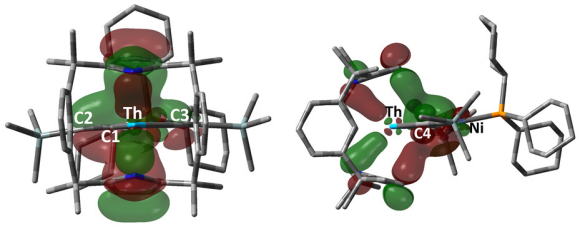

Figure 8. Upper: Selected MOs of complexes **15a** and **15b**. Energies are plotted relative to MO 255 in the $\eta^5{:}\eta^5$ conformation. Hydrogens omitted for clarity. Isovalue = 0.025. Lower: Two expansions of MO 255 in **15a** visualising the two significant bonding interactions contributing to the $\eta^5{:}\eta^5$ conformation stability, isovalues of 0.0275 and Z-clipping, the front view on the left, side view on the right side. (Images have been edited to omit contributions from the SiMe3 groups for clarity.

The MOs labelled in green (MO 265) also feature Ni–alkynyl bonding, but this time the π-orbitals of the two alkynyl ligands are out of phase with each other. MO 265 is more stable in **15b** than in **15a**, and its character doesn't split from one conformation to the other. We attribute its destabilisation from **b** to **a** to a small admixture of L ring π-character. In **15b** this comes from the arene rings while in **15a** it is from the pyrrolides. In isolated $(L)^{2-}$ fragments, these π MOs are 223.1 kJ mol^{-1} less stable in the pyrrolide rings, and so only a small admixture of this character into MO 265 will produce the 35.8 kJ mol^{-1} destabilisation from **15b** to **15a**.

Whilst recognising that there are many other MOs in these compounds, those shown in Figure 8 change by the largest amount between the **a** and **b** forms; hence the likely driver for the greater stability of the $\eta^5{:}\eta^5$ mode is the formation of MO 255.

The analogous MO diagram for **16** is shown in Figure 10. The orbitals labelled in red display very similar behaviour to those of **15a** and **15b** in Figure 8, as evidenced by their energy changes and isosurfaces (Fig. S13 of the SI).

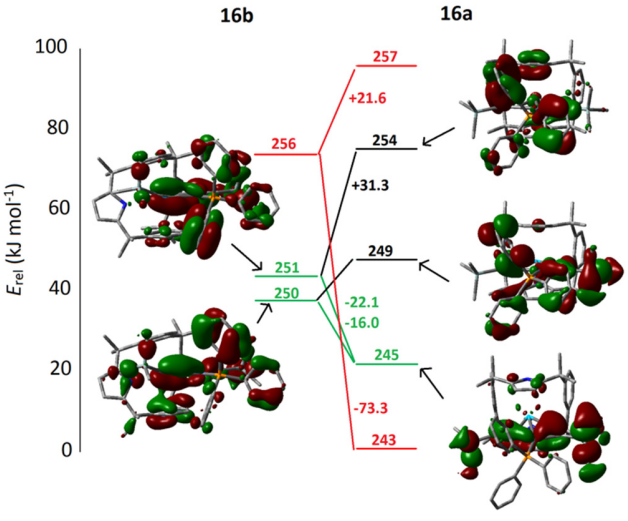

Figure 9. Selected MOs of complexes **16a** and **16b**. Energies are plotted relative to MO 243 in the η^5:η^5 conformation. Hydrogens omitted for clarity. Isovalue = 0.025.

The orbitals labelled in green, however, show different behaviour from those in **15a** and **15b**. For **16b** there are now two Ni–alkynyl bonding interactions in which the alkynyl ligands are out of phase with each other (MOs 250 and 251). This distribution over two MOs arises because these also feature contributions from π-orbitals on the Ph rings of the phosphine, character which obviously cannot be present in the saturated PCy_3 system. The character of **16b**'s MOs 250 and 251 is distributed amongst three MOs in **16a** (245, 249 and 254). There is now only one MO with Ni-alkynyl character (MO 245 - still labelled in green). This is stabilised *vs* MOs 250 and 251 of **16b**, and loses its contribution from the Ph rings. The latter character is now found in **16a** MOs 249 and 254. These are labelled in black in Figure 9 to highlight that they have no Ni-alkynyl character, and are both destabilised *vs* MOs 250 and 251 of **16b**.

As for compounds **15a** and **15b**, Figure 9 suggests that the driver for the greater stability of the η^5:η^5 mode in **16** is the formation of MO 243. It is also tempting to suggest that the slightly larger preference for the **a** conformation in the PPh_3 system is a result of the different behaviour of the orbitals labelled in green in Figures 8 and 9.

Discussion of $(L)^{2-}$ Ligand Conformation. The DFT calculations find that the **a** (η^5:η^5) conformer is the more energetically favoured for both complexes **15** and **16**. This is in agreement with low temperature NMR spectral studies on complex **16**. We recalculated the energies presented in Table 1 for **15** and **16** in the presence of a continuum solvent of THF or hexane. These were found to differ from each other, and from the gas phase data in Table 1, by no more than 2.2 kJ mol^{-1} for **15** and 1.6 kJ mol^{-1} for **16**, showing that the **a** conformer remains the more stable in solution, in agreement with the NMR data for **16**.

It therefore remains unclear how structural isomer **b** forms. **15b** may be a minor product in the reaction mixture that is not resolved in the NMR spectrum. **15b** could also be the result of a packing effect imparted by lattice solvent and formed over several days in a slow rearrangement. Perhaps fluxionality would be promoted at higher temperatures, however complexes **15** and **16** readily decompose in solution when heated, precluding high temperature NMR studies.

CONCLUSIONS

A series of new Th^{IV} and U^{IV} complexes supported by a *trans*-calix[2]benzene[2]pyrrolide ligand have been synthesised, enabling us to demonstrate the flexibility and range of binding modes available to this ligand system, which allows facile incorporation and abstraction of cations in the bis(arene) pocket. This ligand system has shown reversible C–H bond activation chemistry facilitated by its non-innocence and formed an excellent new route to new alkynyl complexes, and alkyl cations of Th^{IV}. Additionally, interesting new bimetallic complexes incorporating nickel were isolated as two conformers **a** (η^5:η^5) and **b** (η^6:κ^1:η^6:κ^1); the first instance of two structural isomers of $(L)^{2-}$ in the same complex. No Th-Ni bond was sought in these ligand-bridged complexes, although the Th-Ni distances are the shortest yet reported, and are significantly shorter than the summed covalent radii.

In reactions with CO_2, the thorium bis(alkynyl) complex cleanly and quantitatively cleaves one CO bond of the small molecule, eventually releasing what is presumed to be thorium oxide, but showing a remarkably selective C-N and C-C bond formation in the insertion of the remaining CO atoms of CO_2 into the macrocycle.

DFT calculations show that the **a** (η^5:η^5) bonding mode of the ancillary $(L)^{2-}$ ligand is favoured, independent of the transition metal (Ni or Pt). Analysis of the Ni systems shows that this preference is due to favourable mixing of a Th-pyrrolide π-bonding orbital with a Ni–alkynyl interaction; this is worth over 70 kJ mol^{-1} in both **15** and **16**. A more tentative orbital-based explanation for the slightly larger preference of the PPh_3 system for the **a** conformation focuses on the involvement of Ph π-orbitals in the Ni-alkynyl interaction, a mixing which cannot occur in the PCy_3 compounds.

EXPERIMENTAL SECTION

General Procedures and Techniques. Standard high-vacuum Schlenk-line techniques and Vac and MBraun glove boxes were used to manipulate and store air- and moisture-sensitive compounds under an atmosphere of dried and deoxygenated dinitrogen. All gases were supplied by BOC gases UK. All glassware was dried in an oven at 160 °C, cooled under 10^{-3} mbar vacuum and then purged with nitrogen. Prior to use, all Fisherbrand® 1.2 µm retention glass microfiber filters and cannulae were dried in an oven at 160 °C overnight and all Celite® 545 filter aid was flame dried under vacuum. All solvents for use with air- and moisture-sensitive compounds were stored in ampoules containing predried 4 Å molecular sieves from the Vac Atmospheres solvent tower drying system, where they had been passed over a column of molecular sieves for 24 hours prior to collection. They were then degassed prior to use and subsequent storage. The solvents benzene-d_6, toluene-d_8, THF-d_8 and pyridine-d_5 were heated under reflux over the appropriate drying agent for 24 hours, vacuum transferred into ampoules and stored under an atmosphere of nitrogen prior to use. All solvents were purchased from Sigma-Aldrich or Fisher Scientific. All NMR spectroscopic analyses were recorded at 298 K using Bruker Avance III 500.12 MHz spectrometers with ^{1}H NMR spectra run at 500.12 MHz, ^{13}C NMR spectra at 125.77 MHz, ^{7}Li NMR spectra run at 194.41 MHz, ^{11}B NMR spectra at 160.49 MHz and ^{29}Si NMR spectra at 99.37 MHz. $SiMe_4$, BF_3·(OEt_2) and LiCl were used to externally reference the relevant spectra. The ^{1}H NMR and ^{13}C{^{1}H} NMR spectra were referenced internally to residual protio solvent (^{1}H) or solvent (^{13}C) and are reported to tetramethylsilane (δ = 0 ppm). Chemical shifts are quoted in δ (ppm) and coupling constants in Hz. Elemental analyses were performed by Mr. Stephen Boyer at the London Metropolitan University. All FTIR spectra were recorded using JASCO 410 or JASCO 460 plus spectrometers. The compounds KCH_2Ph,[81] $LiCH_2SiMe_3$,[82] KN□,[83] $ThCl_4(DME)_2$,[84] *trans*-calix[2]benzene[2]pyrrole (H_2L),[85] K_2L,[70] [$LThCl_2$] (**A**),[29] $KCH(SiMe_3)_2$,[86] were synthesised according to literature procedures.

[(L)UCl_2] (1). A Teflon-valved ampoule with a magnetic stirrer-bar was charged with $UCl_4(THF)_{0.75}$ (0.601 g, 1.38 mmol) and K_2L (0.730 g, 1.38 mmol). THF (40 ml) was added, and the reaction was then stirred and heated at 80 °C for 48 hours. The resulting dark orange solution was cannula-filtered to remove KCl and the vola-

tiles were subsequently removed under reduces pressure. The solids were washed with hexane (3 x 10 ml) and dried under vacuum to yield **1** as an orange solid. Single crystals suitable for X-ray were grown by vapour diffusion of hexane into a saturated solution of **1** in THF at ambient temperature. Yield: 0.772 g (1.02 mmol), 74%. ^{1}H NMR (benzene-d_6): δ 101.07 (s, 4H, pyrrolide C<u>H</u>), 25.93 (s, 12H, C<u>H</u>$_3$), 5.56 (s, 12H, C<u>H</u>$_3$), 10.23 (s, 4H, *meta*-C_6H_4), 14.62 (s, 2H, *para*-C_6H_4). 2H on *ipso*-C_6H_4 were not observed. Analysis (%) calc. for $C_{32}H_{36}N_2Cl_2U$: C 50.73; H 4.79; N 3.70, found C 50.86; H 4.74; N 3.83.

Li[(L^{-2H})Th(Me)] (2). A Teflon-valved ampoule with a magnetic stirrer-bar was charged with **A** (1.50 g, 2.00 mmol) and LiMe (3eq, 0.132 g, 6.00 mmol). THF was added (20 ml), the reaction sonicated for 15 minutes and stirred for 16 hours. The resulting yellow solution was cannula-filtered to remove LiCl. The volatiles were then removed under reduced pressure and the solids dried under vacuum to yield **2** as a pale yellow solid. Single crystals suitable for X-ray were grown by vapour diffusion of hexane into a saturated THF solution of **2** at ambient temperature. Yield: 1.30 g (1.86 mmol), 93%. ^{1}H NMR (THF-d_8): δ 6.96 (d, $|^3J_{HH}|$ = 7.65 Hz, 4H, *meta*-C_6H_3), 6.84 (t, $|^3J_{HH}|$ = 7.69 Hz, 2H, *para*-C_6H_3), 6.44 (s, 4H, pyrrolide C<u>H</u>), 1.58 (s, 12H, *exo*-C<u>H</u>$_3$), 1.41 (s, 12H, *endo*-C<u>H</u>$_3$), -0.73 (s, 3H, Th-C<u>H</u>$_3$). ^{13}C{^{1}H} NMR (THF-d_8): δ 217.6 (Th-<u>C</u>), 167.2 (quaternary aromatic), 159.2 (quaternary aromatic), 125.7 (*para*-C_6H_3), 121.7 (*meta*-C_6H_3), 115.7 (pyrrolide <u>C</u>H), 54.1 (Th-<u>C</u>H$_3$), 45.3 (quaternary), 35.2 (<u>C</u>H$_3$), 31.7 (<u>C</u>H$_3$). ^{7}Li{^{1}H} NMR (THF-d_8): δ 0.15. Analysis (%) calc. for $C_{41}H_{53}N_2O_2LiTh$ (Li[(L^{-2H})Th(Me)]·2THF): C 58.29; H 6.32; N 3.32, found C 58.45; H 6.46; N 3.22.

Li[(L^{-2H})Th(CH$_2$SiMe$_3$)](3). A Teflon-valved ampoule with a magnetic stirrer-bar was charged with **A** (1.28 g, 1.70 mmol) and LiCH$_2$SiMe$_3$ (3eq, 0.481 g, 5.11 mmol). Toluene was added (20 ml), the reaction sonicated for 15 minutes and then stirred for 16 hours. The resulting yellow solution was cannula-filtered to remove LiCl and the volatiles were removed under reduced pressure. The solids were washed with hexane (3 x 5 ml) and then dried under vacuum to yield **3** as a pale yellow solid. Single crystals suitable for X-ray were grown in the presence of LiCl by vapour diffusion of hexane into a saturated THF solution of **3** at ambient temperature. Yield: 0.958 g (1.24 mmol), 73%. ^{1}H NMR (benzene-d_6): δ 7.29 (t, $|^3J_{HH}|$ = 6.77 Hz, 2H, *para*-C_6H_3), 7.22 (d, $|^3J_{HH}|$ = 7.58 Hz, 4H, *meta*-C_6H_3), 6.83 (s, 4H, pyrrolide C<u>H</u>), 1.61 (s, 12H, *exo*-C<u>H</u>$_3$), 1.57 (s, 12H, *endo*-C<u>H</u>$_3$), 0.35 (s, 9H, Si(C<u>H</u>$_3$)$_3$), -0.16 (s, 2H, Th-C<u>H</u>$_2$). ^{13}C{^{1}H} NMR (benzene-d_6): δ 213.6 (Th-<u>C</u>), 165.3 (quaternary aromatic), 159.2 (quaternary aromatic), 125.7 (*meta*-C_6H_3), 123.4 (*para*-C_6H_3), 115.5 (pyrrolide <u>C</u>H), 44.5 (quaternary), 35.5 (<u>C</u>H$_3$), 31.1 (<u>C</u>H$_3$), 25.2 (Th-<u>C</u>H$_2$), 4.9 (Si(<u>C</u>H$_3$)$_3$). ^{29}Si{^{1}H} NMR (benzene-d_6): δ -0.52 (<u>Si</u>(CH$_3$)$_3$). ^{7}Li{^{1}H} NMR (benzene-d_6): δ -0.24. Analysis (%) calc. for $C_{41}H_{53}N_2O_2LiTh$ (Li[(L^{-2H})Th(CH$_2$SiMe$_3$)]·2THF): C 58.29; H 6.32; N 3.32, found C 58.45; H 6.46; N 3.22.

K[(L^{-2H})Th(CH$_2$Ph)] (4). A Teflon-valved ampoule with a magnetic stirrer-bar was charged with **A** (0.200 g, 0.266 mmol) and KCH$_2$Ph (3eq, 0.104 g, 0.798 mmol). Toluene was added (20 ml) and the reaction sonicated for 15 minutes and stirred for 16 hours. The resulting orange solution was cannula-filtered to remove KCl and the volatiles were removed under reduced pressure. The solids were washed with hexane (3 x 5 ml) and then dried under vacuum to yield **4** as a pale orange solid. Single crystals suitable for X-ray were grown by vapour diffusion of hexane into a saturated THF solution of **4** at ambient temperature. Yield: 0.152 g (0.188 mmol), 71%. ^{1}H NMR (benzene-d_6): δ 7.30 (m, 4H, *meta*-C_6H_3), 7.15-6.99 (m, 3H, *para*-C_6H_3 and *meta*-C_6H_5), 6.94 (d, $|^3J_{HH}|$ = 7.32 Hz, 2H, *ortho*-C_6H_5), 6.84 (t, $|^3J_{HH}|$ = 6.90 Hz, 1H, *para*-C_6H_5), 6.38 (s, 4H, pyrrolide C<u>H</u>), 1.91 (s, 2H, Th-C<u>H</u>$_2$), 1.63 (s, 12H, *exo*-C<u>H</u>$_3$), 1.49 (s, 12H, *endo*-C<u>H</u>$_3$). ^{13}C{^{1}H} NMR (benzene-d_6): δ 215.8 (Th-<u>C</u>), 166.8 (quaternary aromatic), 160.4 (quaternary aromatic), 151.5 (quaternary aromatic), 128.6 (*meta*-C_6H_3), 126.1, 125.7 (*para*-C_6H_3 and *meta*-C_6H_5), 125.0 (*ortho*-C_6H_5), 119.0 (*para*-C_6H_5), 115.7 (pyrrolide <u>C</u>H), 67.4 (Th-<u>C</u>H$_2$) 45.3 (quaternary), 34.5 (<u>C</u>H$_3$), 30.5 (<u>C</u>H$_3$). Analysis (%) calc. for $C_{39}H_{41}N_2KTh$: C 57.91; H 5.11; N 3.46, found C 58.08; H 5.23; N 3.32.

Li[(L^{-2H})U(Me)] (5). A Teflon-valved ampoule with a magnetic stirrer-bar was charged with **1** (0.900 g, 0.957 mmol) and LiMe (3eq, 0.063 g, 2.87 mmol). THF was added (20 ml), the reaction sonicated for 15 minutes and stirred for 16 hours. The resulting dark brown solution was cannula-filtered to remove LiCl. The volatiles were then removed under reduced pressure and the solids dried under vacuum to yield **5** as a dark orange solid. Yield: 0.653 g (0.924 mmol), 97%. ^{1}H NMR (THF-d_8): δ 84.4 (s, 4H, pyrrolide C<u>H</u>), 12.8 (s, 12H, C<u>H</u>$_3$), 5.18 (s, 12H, C<u>H</u>$_3$), -2.68 (s, 5H, U-C<u>H</u>$_3$ and C_6H_3), -3.84 (s, 4H, C_6H_3). ^{13}C{^{1}H} NMR (benzene-d_6): δ 150.1 (aromatic), 129.3 (aromatic), 128.6 (aromatic), 125.7 (aromatic), 104.2 (aromatic), 67.9 (quaternary aliphatic), 55.9 (U-<u>C</u>H$_3$), 24.8 (<u>C</u>H$_3$), 19.7 (<u>C</u>H$_3$). *Ipso*-<u>C</u>$_6$H$_3$ could not be assigned. ^{7}Li{^{1}H} NMR (benzene-d_6): δ -36.0. Analysis (%) calc. for $C_{33}H_{37}N_2LiU$: C 56.09; H 5.28; N 3.96, found C 56.22; H 5.37; N 3.74.

Li[(L^{-2H})U(CH$_2$SiMe$_3$)] (6). A Teflon-valved ampoule with a magnetic stirrer-bar was charged with **1** (0.030 g, 0.039 mmol) and LiCH$_2$SiMe$_3$ (3eq, 0.011 g, 0.180 mmol). Benzene-d_6 was added (1 ml), the reaction sonicated for 20 minutes and left to react for 16h. The resulting dark brown solution was centrifuged and glass-filtered to remove LiCl and the volatiles were removed under reduced pressure. The solids were dried under vacuum to yield **6** as a dark orange solid. Single crystals suitable for X-ray were grown in the presence of LiCl by vapour diffusion of hexane into a saturated THF solution of **7** at ambient temperature. Yield: 0.020 g (0.026 mmol), 65%. ^{1}H NMR (benzene-d_6): δ 88.7 (s, 4H, pyrrolide C<u>H</u>), 18.5 (s, 12H, C<u>H</u>$_3$), -2.69 (s, 12H, C<u>H</u>$_3$), -3.93 - -8.17 (m, 6H, *meta*-C_6H_3 and *para*-C_6H_3), -12.9 (s, 2H, U-C<u>H</u>$_2$), -27.9 (s, 9H, Si(C<u>H</u>$_3$)$_3$). ^{13}C{^{1}H} NMR (benzene-d_6): δ 151.1 (aromatic), 147.5 (aromatic), 124.2 (aromatic), 122.5 (aromatic), 102.4 (aromatic), 68.2 (quaternary aliphatic), 40.5 (<u>C</u>H$_3$), 31.7 (<u>C</u>H$_3$), 25.5 (U-<u>C</u>H$_2$), 1.43 (Si-<u>C</u>H$_3$). *Ipso*-<u>C</u>$_6$H$_3$ could not be assigned. ^{29}Si{^{1}H} NMR (benzene-d_6): Resonance could not be found. ^{7}Li{^{1}H} NMR (benzene-d_6): δ -52.7. Analysis (%) calc. for $C_{36}H_{45}N_2LiSiU$: C 55.52; H 5.82; N 3.60, found C 55.48; H 5.63; N 3.71.

K[(L^{-2H})U(CH$_2$Ph)] (7). A Teflon-valved ampoule with a magnetic stirrer-bar was charged with **1** (0.100 g, 0.132 mmol) and KCH$_2$Ph (3eq, 0.052 g, 0.396 mmol). Toluene was added (20 ml) and the reaction sonicated for 15 minutes and stirred for 16 hours. The resulting dark brown solution was cannula-filtered to remove KCl and the volatiles were removed under reduced pressure. The solids were washed with hexane (3 x 5 ml) and then dried under vacuum to yield **7** as a dark orange solid. Yield: 0.050 g (0.061 mmol), 46 %. ^{1}H NMR (benzene-d_6): δ 97.8 (s, 4H, pyrrolide C<u>H</u>), 28.6 (s, 12H, C<u>H</u>$_3$), 11.2 (s, 2H, *para*-C_6H_3), -4.42 (s, 4H, *meta*-C_6H_3), -4.76 (s, 2H, *para*-C_6H_5), -5.62 (m, 4H, *ortho*-C_6H_5 and *meta*-C_6H_5), -6.58 (s, 12H, C<u>H</u>$_3$), -57.8 (v br s, 2H, U-C<u>H</u>$_2$). ^{13}C{^{1}H} NMR (benzene-d_6): δ 225.8 (quaternary aromatic), 144.6 (aromatic), 142.0 (aromatic), 128.8 (aromatic), 128.6 (aromatic), 126.2 (aromatic), 122.7 (aromatic), 121.2 (aromatic), 113.3 (aromatic), 67.1 (quaternary aliphatic), 38.2 (<u>C</u>H$_3$), 30.0 (<u>C</u>H$_3$), 25.5 (U-<u>C</u>H$_2$). One aromatic resonance is obscured by the solvent peak and could not be assigned. Analysis (%) calc. for $C_{39}H_{41}N_2KU$: C 57.48; H 5.07; N 3.44, found C 57.60; H 5.00; N 3.34.

[(L)Th(C≡CSiMe$_3$)$_2$] (8). A Teflon-valved ampoule with a magnetic stirrer-bar was charged with **2** (1.00 g, 1.43 mmol) and HC≡CSiMe$_3$ (2eq, 0.280 g, 2.86 mmol). Hexane was added (30 ml) and the reaction was stirred for 3 hours. The hexane solution of **8** was filtered away from the solids, the volatiles were removed under reduced pressure and the solids were then dried under vacuum to yield **8** as yellow solid. Single crystals suitable for X-ray were grown from a saturated solution of benzene at ambient temperature. Yield: 0.544 g (0.622 mmol), 44%. ^{1}H NMR (benzene-d_6): δ 7.96 (s, 2H, *ipso*-C_6H_4), 7.51 (s, 4H, pyrrolide C<u>H</u>), 7.09 (d, $|^3J_{HH}|$ = 7.01 Hz, 4H, *meta*-C_6H_4), 7.02 (t, $|^3J_{HH}|$ = 8.00 Hz, 2H, *para*-C_6H_4), 1.92 (s, 12H, C<u>H</u>$_3$), 1.51 (s, 12H, C<u>H</u>$_3$), 0.28 (s, 18H, Si(C<u>H</u>$_3$)$_3$).

$^{13}C\{^1H\}$ NMR (benzene-d_6): δ 188.7 (Th-C), 155.4 (quaternary aromatic), 152.9 (quaternary aromatic), 133.7 (*para*-C_6H_4), 123.9 (*ipso*-C_6H_4), 123.7 (*meta*-C_6H_4), 119.4 (pyrrolide CH), 41.9 (quaternary), 30.3 (CH_3), 27.8 (CH_3), 0.58 ($Si(CH_3)_3$). $^{29}Si\{^1H\}$ NMR (benzene-d_6): δ -24.7. Analysis (%) calc. for $C_{42}H_{54}N_2Si_2Th$: C 57.65; H 6.22; N 3.20, found C 57.51; H 6.33; N 2.98. FTIR (cm^{-1}): 2140 [C≡C stretch].

[(L)Th(C≡CSi^{i}Pr$_3$)$_2$] (9). A Teflon-valved ampoule with a magnetic stirrer-bar was charged with **2** (0.100 g, 0.143 mmol) and HC≡CSi^{i}Pr$_3$ (2eq, 0.052 g, 0.286 mmol). Hexane was added (10 ml) and the reaction was stirred for 3 hours. The hexane solution of **9** was filtered away from the solids, the volatiles were removed under reduced pressure and the solids were then dried under vacuum to yield **9** as yellow solid. Single crystals suitable for X-ray were grown from a saturated solution of benzene at ambient temperature. Yield: 0.080 g (0.077 mmol), 54%. ^1H NMR (benzene-d_6): δ 7.90 (s, 2H, *ipso*-C_6H_4), 7.53 (s, 4H, pyrrolide CH), 7.10 (d, $|^3J_{HH}|$ = 7.70 Hz, 4H, *meta*-C_6H_4), 7.02 (t, $|^3J_{HH}|$ = 7.70 Hz, 2H, *para*-C_6H_4), 1.97 (s, 12H, CH_3), 1.52 (s, 12H, CH_3), 1.35 (d, $|^3J_{HH}|$ = 7.20 Hz, 36H, $SiCH(CH_3)_2$, 1.22 (septet, $|^3J_{HH}|$ = 7.20 Hz, 6H, SiCH). $^{13}C\{^1H\}$ NMR (benzene-d_6): δ 190.04 (Th-C), 155.4 (quaternary aromatic), 152.9 (quaternary aromatic), 133.6 (*para*-C_6H_4), 123.7 (*ipso*-C_6H_4 and *meta*-C_6H_4), 119.0 (pyrrolide CH), 41.9 (quaternary), 30.3 (CH_3), 28.0 (CH_3), 19.4 ($SiCH(CH_3)_2$), 12.3 (SiCH). $^{29}Si\{^1H\}$ NMR (benzene-d_6): δ -6.83. Analysis (%) calc. for $C_{54}H_{78}N_2Si_2Th$: C 62.16; H 7.54; N 2.68, found C 62.33; H 7.62; N 2.46. FTIR (cm^{-1}): 2032 [C≡C stretch].

[(L)U(C≡CSiMe$_3$)$_2$] (10). A Teflon-valved ampoule with a magnetic stirrer-bar was charged with **5** (0.050 g, 0.071 mmol) and HC≡CSiMe$_3$ (2eq, 0.014 g, 0.142 mmol). Hexane was added (3 ml) and the reaction was stirred for 3 hours. The hexane solution of **10** was filtered away from the solids, the volatiles were removed under reduced pressure and the solids were then dried under vacuum to yield **10** as orange solid. Yield: 0.031 g (0.035 mmol), 50 %. ^1H NMR (THF-d_6): δ 92.8 (s, 4H, pyrrolide CH), 26.6 (s, 12H, CH_3), -6.11 (s, 12H, CH_3), -10.2 (s, 4H, *meta*-C_6H_4), -12.7 (m, 2H, C_6H_4), -13.9 (s, 18H, $Si(CH_3)_3$), -14.4 (s, 2H, C_6H_4). $^{29}Si\{^1H\}$ NMR (benzene-d_6): δ 34.5. Analysis (%) calc. for $C_{42}H_{54}N_2Si_2U$: C 57.25; H 6.18; N 3.18, found C 57.32; H 6.05; N 3.11.

[(L)U(C≡CSi^{i}Pr$_3$)$_2$] (11). A Teflon-valved ampoule with a magnetic stirrer-bar was charged with **5** (0.100 g, 0.142 mmol) and HC≡CSi^{i}Pr$_3$ (2eq, 0.052 g, 0.284 mmol). Hexane was added (10 ml) and the reaction was stirred for 3 hours. The hexane solution of **11** was filtered away from the solids, the volatiles were removed under reduced pressure and the solids were then dried under vacuum to yield **11** as orange solid. Single crystals suitable for X-ray were grown from a saturated solution of benzene at ambient temperature. Yield: 0.074 g (0.071 mmol), 50 %. ^1H NMR (benzene-d_6): δ 92.5 (s, 4H, pyrrolide CH), 26.3 (s, 12H, CH_3), -6.00 (s, 12H, CH_3), -9.50 (m, 38H, ^{i}Pr-CH_3 and C_6H_4), -10.2 (s, 4H, *meta*-C_6H_4), -12.7 (septet, $|^3J_{HH}|$ = 7.25 Hz, 6H, ^{i}Pr-CH), -14.1 (s, 2H, C_6H_4). $^{29}Si\{^1H\}$ NMR (benzene-d_6): δ -21.9. Analysis (%) calc. for $C_{54}H_{78}N_2Si_2U$: C 61.80; H 7.49; N 2.67, found C 62.07; H 7.34; N 2.83. FTIR (cm^{-1}): 2032 [C≡C stretch].

[(L)Th(CH$_2$Ph)][BPh$_4$] (12). A Teflon-valved ampoule with a magnetic stirrer-bar was charged with **4** (0.040 g, 0.050 mmol) and $[Et_3NH][BPh_4]$ (2eq, 0.042 g, 0.100 mmol). THF was added (2 ml) and the resulting suspension was stirred for 2 hours. The pale yellow solution was then cannula-filtered to remove $KBPh_4$. The volatiles were removed under reduced pressure and the solids were then dried under vacuum to yield **12** as off-white solid. Material sufficiently pure for elemental analysis could not be obtained. Yield: 0.017 g (0.016 mmol), 31%. ^1H NMR (THF-d_8): δ 7.72 (s, 2H, *ipso*-C_6H_4), 7.40-7.08 (m, 19H, aromatic-H), 7.00 (s, 4H, pyrrolide CH), 6.85 (t, $|^3J_{HH}|$ = 7.28 Hz, 8H, *meta*-C_6H_5), 6.71 (t, $|^3J_{HH}|$ = 6.92 Hz, 4H, *para*-C_6H_5), 2.89 (s, 2H, Th-CH_2), 1.79 (s, 12H, CH_3), 1.47 (s, 12H, CH_3). $^{13}C\{^1H\}$ NMR (THF-d_8): δ 158.3 (quaternary aromatic), 153.9 (aromatic-C_6H_5), 153.2 (aromatic-C_6H_5), 137.3 (tetraphenyl borate *meta*-C_6H_5), 134.9 (quaternary aromatic), 129.1 (*ipso*-C_6H_4), 128.8 (aromatic-C_6H_5), 128.4 (aromatic-C_6H_5), 126.7 (*para*-C_6H_4), 125.8 (tetraphenyl borate *ortho*-C_6H_5), 123.9 (pyrrolide CH), 123.3 (*meta*-C_6H_4), 121.9 (tetraphenyl borate *para*-C_6H_5), 42.6 (quaternary), 30.9 (CH_3), 30.8 (Th-CH_2) 28.0 (CH_3). $^{11}B\{^1H\}$ NMR (THF-d_8): δ -6.56.

[(L)Th(N(SiMe$_3$)$_2$)][BPh$_4$] (13). A Teflon-valved ampoule with a magnetic stirrer-bar was charged with **C** (0.500 g, 0.570 mmol) and $[Et_3NH][BPh_4]$ (2eq, 0.480 g, 1.140 mmol). THF was added (30 ml) and the resulting suspension was stirred for 2 hours. The grey solution was then cannula-filtered to remove $KBPh_4$. The volatiles were removed under reduced pressure and the solids were then dried under vacuum to yield **13** as a grey solid. Single crystals suitable for X-ray were grown by vapour diffusion of hexane into a saturated THF solution of **13** at ambient temperature. Yield: 0.449 g (0.387 mmol), 68%. ^1H NMR (THF-d_8): δ 8.23 (s, 2H, *ipso*-C_6H_4), 8.04 (d, $|^3J_{HH}|$ = 1.54 Hz, 4H, *meta*-C_6H_4), 7.26 (m, 8H, *ortho*-C_6H_5), 7.15 (m, 2H, *para*-C_6H_4), 6.85 (t, $|^3J_{HH}|$ = 7.47 Hz, 8H, *meta*-C_6H_5), 6.70 (t, $|^3J_{HH}|$ = 7.19 Hz, 4H, *para*-C_6H_5), 6.15 (s, 4H, pyrrolide CH), 1.78 (s, 12H, CH_3), 1.63 (s, 12H, CH_3), 0.14 (s, 18H, $Si(CH_3)_3$). $^{13}C\{^1H\}$ NMR (THF-d_8): δ 158.3 (quaternary aromatic), 157.2 (quaternary aromatic), 137.3 (tetraphenyl borate *meta*-C_6H_5), 132.4 (*ipso*-C_6H_4), 127.8 (*para*-C_6H_4), 126.0 (tetraphenyl borate *ortho*-C_6H_5), 122.4 (*meta*-C_6H_4), 122.1 (tetraphenyl borate *para*-C_6H_5), 107.4 (pyrrolide CH), 42.7 (quaternary), 33.4 (CH_3), 29.3 (CH_3), 4.1 ($Si(CH_3)_3$). $^{29}Si\{^1H\}$ NMR (THF-d_8): δ -12.4. $^{11}B\{^1H\}$ NMR (THF-d_8): δ -6.57. Analysis (%) calc. for $C_{62}H_{74}BN_3Si_2Th$: C 64.18; H 6.43; N 3.62, found C 64.26; H 6.34; N 3.55.

[LCO] (14). A Young's tube was charged with **8** (0.050 g, 0.057 mmol) or **10** (0.050 g, mmol) in C_6D_6 (1 ml), 1 bar of CO_2 added and the reaction vessel heated at 80 °C for 16 hours. Off-white solids formed and were filtered away from the solution containing **14**. The volatiles were removed under reduced pressure and the solids then dried under vacuum to yield 1^{10},1^{10},2,2,4,4,6,6-octamethyl-1^5,1^{10}-dihydro-3^1*H*-1(6,3)-pyrrolo[1,2-*b*]isoquinolina-3(2,5)-pyrrola-5(1,3)-benzenacyclohexaphan-1^5-one, LCO **14** as a colourless solid. Single crystals suitable for X-ray were grown from a saturated solution of **14** in hexane at -20 °C. Yield: 0.019 g (0.040 mmol), 70 %. ^1H NMR (benzene-d_6): δ 7.41 (m, 1H, arene-H), 7.32-7.25 (m, 3H, arene-H), 7.08 (m, 1H, arene-H), 6.98 (m, 1H, arene-H), 6.90 (m, 1H, arene-H), 6.34 (m, 1H, pyr-CH), 5.92 (m, 2H, pyr-CH), 5.23 (m, 1H, pyr-CH), 3.86 (br. s, 1H, pyr-NH), 1.75 (br. s, 12H, CH_3), 1.60 (s, 6H, CH_3), 1.34 (s, 6H, CH_3). $^{13}C\{^1H\}$ NMR (benzene-d_6): δ 159.4 (C=O), 156.5 (quaternary arene), 149.4 (quaternary arene), 149.0 (quaternary arene), 148.7 (quaternary arene), 143.3 (quaternary arene), 143.0 (quaternary arene), 142.6 (quaternary arene), 138.7 (quaternary arene), 131.1 (arene-CH), 129.1 (arene-CH), 129.0 (quaternary arene), 126.5 (arene-CH), 124.8 (arene-CH), 123.7 (arene-CH), 123.2 (arene-CH), 121.0 (arene-CH), 115.7 (pyr-CH), 106.3 (pyr-CH), 104.9 (pyr-CH), 103.4 (pyr-CH), 44.5 (CH_3), 41.6 (CH_3), 39.5 (CH_3), 37.4 (CH_3), 30.4 (quaternary), 29.6 (quaternary), 25.8 (quaternary). Analysis (%) calc. for $C_{33}H_{36}N_2O$: C 83.15; H 7.61; N 5.88, found C 83.06; H 7.69; N 5.93.

[(L)Th(C≡CSiMe$_3$)$_2$][NiPCy$_3$] (15a and 15b). A Teflon-valved ampoule with a magnetic stirrer-bar was charged with **9** (0.100 g, 0.114 mmol), $[Ni(COD)_2]$ (1eq, 0.031 g, 0.114 mmol) and PCy_3 (1eq, 0.032 g, 0.114 mmol). Hexane was added (5 ml) and the reaction was stirred for 3 hours. The volatiles were removed under reduced pressure and the solids were then dried under vacuum to yield **15** as dark orange solid. Single crystals suitable for X-ray were grown by two different methods: vapour diffusion of hexane into a saturated THF solution of **15** at ambient temperature to yield **15a** and slow evaporation of from a saturated solution of **15** in hexane to yield **15b**. Yield of **15a**: 0.010 g (0.008 mmol), 7 %. Yield of **15b**: 0.006 g (0.005 mmol), 4 %. ^1H NMR (benzene-d_6): δ 8.22 (s, 2H, *ipso*-C_6H_4), 7.29 (m, 2H, *para*-C_6H_4), 7.22 (m, 4H, *meta*-C_6H_4), 6.39 (s, 4H, pyrrolide CH), 2.46-2.11 (m, 33H, Cy-H), 1.79 (s, 12H, *exo*-CH_3), 1.64 (s, 12H, *endo*-CH_3), 0.28 (s, 18H, $Si(CH_3)_3$). $^{13}C\{^1H\}$

NMR (benzene-d_6): δ 158.0 (quaternary aromatic), 152.9 (quaternary aromatic), 134.0 (*para*-C_6H_4), 132.0 (*ipso*-C_6H_4), 131.5 (*meta*-C_6H_4), 114.1 (pyrrolide C<u>H</u>), 68.2 (C≡C), 42.2 (<u>C</u>H_3), 42.0 (quaternary), 36.6 (d, $|^1J_{PC}|$ = 12.7 Hz, P-C_6H_{11}), 33.8 (C≡C), 30.8 (d, $|^2J_{PC}|$ = 1.34 Hz, P-C_6H_{11}), 29.3 (<u>C</u>H_3), 28.0 (P-C_6H_{11}), 27.3 (P-C_6H_{11}), 25.6 (Si(<u>C</u>H_3)$_3$). $^{29}Si\{^1H\}$ NMR (benzene-d_6): δ -17.6. $^{31}P\{^1H\}$ NMR (benzene-d_6): δ 49.2. Analysis (%) calc. for $C_{60}H_{87}N_2Si_2PNiTh$: C 59.35; H 7.22; N 2.31, found C 59.15; H 7.05; N 2.39.

[(L)Th(C≡CSiMe$_3$)$_2$][NiPPh$_3$] (16). A Teflon-valved ampoule with a magnetic stirrer-bar was charged with **9** (0.100 g, 0.114 mmol), [Ni(COD)$_2$] (1eq, 0.031 g, 0.114 mmol) and PPh_3 (1eq, 0.030 g, 0.114 mmol). Hexane was added (5 ml) and the reaction was stirred for 3 hours. The volatiles were removed under reduced pressure and the solids were then dried under vacuum to yield **16** as dark orange solid. Single crystals suitable for X-ray were grown by vapour diffusion of hexane into a saturated THF solution of **16** at ambient temperature. Yield: 0.025 g (0.021 mmol), 18 %. ^1H NMR (benzene-d_6): δ 9.09 (s, 2H, *ipso*-C_6H_4), 7.94 (m, 6H, *ortho*-P-C_6H_5), 7.22-7.16 (m, 10H, *meta*-C_6H_4 and *meta*-P-C_6H_5), 7.12 (m, 3H, *para*-P-C_6H_5), 7.04 (m, 2H, *para*-C_6H_4), 6.68 (s, 4H, pyrrolide C<u>H</u>), 1.90 (s, 12H, *exo*-C<u>H</u>$_3$), 1.58 (s, 12H, *endo*-C<u>H</u>$_3$), 0.00 (s, 18H, Si(C<u>H</u>$_3$)$_3$). ^1H NMR (298 K, toluene-d_8): δ 9.03 (s, 2H, *ipso*-C_6H_4), 7.89 (m, 6H, *ortho*-P-C_6H_5), 7.13 (m, 6H, *meta*-P-C_6H_5), 7.06-7.01 (m, 9H, *para*-P-C_6H_5, *meta*-C_6H_4 and *para*-C_6H_4), 6.60 (s, 4H, pyrrolide C<u>H</u>), 1.87 (s, 12H, *exo*-C<u>H</u>$_3$), 1.55 (s, 12H, *endo*-C<u>H</u>$_3$), 0.05 (s, 18H, Si(C<u>H</u>$_3$)$_3$). ^1H NMR (210 K, toluene-d_8): δ 9.77 (s, 1H, *ipso*-C_6H_4), 8.60 (s, 1H, *ipso*-C_6H_4), 7.93 (m, 6H, *ortho*-P-C_6H_5), 7.19-7.04 (m, 15H, *meta*-P-C_6H_5, *para*-P-C_6H_5, *meta*-C_6H_4 and *para*-C_6H_4), 6.77 (br m, 4H, pyrrolide C<u>H</u>), 1.96-1.81 (very br d, 12H, *exo*-C<u>H</u>$_3$), 1.61 (s, 12H, *endo*-C<u>H</u>$_3$), 0.04 (br s, 18H, Si(C<u>H</u>$_3$)$_3$). ^1H NMR (298 K, THF-d_8): δ 8.85 (s, 2H, *ipso*-C_6H_4), 7.72 (m, 6H, *ortho*-P-C_6H_5), 7.36-7.06 (m, 15H, *meta*-C_6H_4, *meta*-P-C_6H_5, *para*-P-C_6H_5 and *para*-C_6H_4), 6.39 (s, 4H, pyrrolide C<u>H</u>), 1.79 (s, 12H, *exo*-C<u>H</u>$_3$), 1.45 (s, 12H, *endo*-C<u>H</u>$_3$), -0.27 (s, 18H, Si(C<u>H</u>$_3$)$_3$). ^1H NMR (193 K, THF-d_8): δ 9.48 (s, 1H, *ipso*-C_6H_4), 8.35 (s, 1H, *ipso*-C_6H_4), 7.80-7.51 (br m, 6H, *ortho*-P-C_6H_5), 7.39-6.98 (br m, 15H, *meta*-C_6H_4, *meta*-P-C_6H_5, *para*-P-C_6H_5 and *para*-C_6H_4), 6.54 (d, 2H, pyrrolide C<u>H</u>), 6.26 (d, 2H, pyrrolide C<u>H</u>), 1.82 (br s, 12H, *exo*-C<u>H</u>$_3$), 1.45 (br s, 12H, *endo*-C<u>H</u>$_3$), -0.27 (s, 9H, Si(C<u>H</u>$_3$)$_3$), -0.36 (s, 9H, Si(C<u>H</u>$_3$)$_3$). $^{13}C\{^1H\}$ NMR (benzene-d_6): δ 157.2 (quaternary aromatic), 153.8 (quaternary aromatic), 139.5 (d, $|^1J_{PC}|$ = 30.7 Hz, *ipso*-P-C_6H_5), 135.0 (d, $|^2J_{PC}|$ = 13.7 Hz, *ortho*-P-C_6H_5), 132.4 (*para*-C_6H_4), 129.3 (d, $|^4J_{PC}|$ = 1.29 Hz, *para*-P-C_6H_5), 128.0 (*meta*-P-C_6H_5), 123.4 (*ipso*-C_6H_4), 123.4 (*meta*-C_6H_4), 114.8 (pyrrolide <u>C</u>H), 42.2 (quaternary), 30.8 (<u>C</u>H_3), 28.9 (<u>C</u>H_3), 23.1 (C≡C), 14.4 (C≡C), 2.53 (Si(<u>C</u>H_3)$_3$). $^{29}Si\{^1H\}$ NMR (benzene-d_6): δ -16.0 (d, $|^4J_{PSi}|$ = 6.68 Hz). ^{31}P NMR (benzene-d_6): δ 37.0 (m). Analysis (%) calc. for $C_{60}H_{69}N_2Si_2PNiTh$: C 60.25; H 5.81; N 2.34, found C 60.49; H 5.73; N 2.30. FTIR (cm^{-1}): 2120 [C≡C stretch], 2071 [C≡C stretch].

Crystallographic Details. X-ray crystallography on compounds **1**, **2**, **3·LiCl**, **4·THF**, **6·LiCl·THF**, **8**, **9**, **11** and **13-16** was completed using an Oxford Diffraction Excalibur Eos diffractometer with Mo Kα radiation at 170(2) K or an Agilent Technologies Supernova dual source Atlas diffractometer using a Cu Kα source at 120(10) K. All structures were solved using SHELXT and least-square refined using SHELXL in Olex2.[87-88]

Computational Methodology. Geometry optimisations, without symmetry constraints, were carried out using Kohn-Sham density functional theory in the Gaussian 09 code (revision D.01)[89], using the PBE0 hybrid functional.[90] Dunning's correlation consistent polarised valence triple-ζ quality basis sets (cc-pVTZ)[91] were used for all light atoms (C, N, Si, and P) – except for hydrogen, for which the polarised valence double-ζ (cc-pVDZ) quality basis set[92] was used. A Stuttgart/Bonn quasi-relativistic 60 electron pseudopotential and associated valence basis sets was used for thorium.[93-94] Fully-relativistic 10 and 60 electron Stuttgart/Bonn pseudopotentials and associated valence basis sets were used for nickel[95-96] and platinum[97] respectively. The ultra-fine integration grid was used. Frequency calculations were used to determine if stationary points were true minima, and to obtain thermodynamic corrections to the self-consistent field (SCF) energies needed for the Gibbs energies. Default SCF and geometry convergence criteria were employed. For calculating the dipole moments in different solvent environments, the polarisable continuum model (PCM) devised by Tomasi, Pascual-Ahuir and coworkers,[98-103] was employed to model the solvation effects on the dipole moment in 15 and 16 in both THF and hexane. The default solvent radius was used.

ASSOCIATED CONTENT

Supporting Information

Figures S1-S7 showing molecular structures of **1**, **3·LiCl**, **6·LiCl·THF**, **9**, **11**, **14**, and **16a**. Tables S1-S5 giving crystal structure and refinement data. Tables S6-S8 showing additional computational data. Figures S8-S12 show NMR spectra for **2**, **8** and **16**. Figure S13 showing additional MOs of 16. List of geometry optimised xyz coordinates.
The Supporting Information is available free of charge on the ACS Publications website.

AUTHOR INFORMATION

Corresponding Author

* E-mail for P.L.A.: polly.arnold@ed.ac.uk
* E-mail for N.K.: nikolas.kaltsoyannis@manchester.ac.uk

Present Address

§School of Chemistry, WestCHEM, University of Glasgow, Glasgow G12 8QQ, United Kingdom

Notes

The authors declare no conflict of interest.

ACKNOWLEDGMENTS

We thank the University of Edinburgh for a Principal's Career Development PhD Scholarship and ScotCHEM International Graduate School Scholarship to M.S.. We are grateful to the University of Manchester for a PhD studentship to K. T. P. O'B., and to the University's Computational Shared Facility for computational resources and associated support. The EPSRC are also thanked for support through grants EP/H004823 1 and EP/N022122/1.

REFERENCES

1. Arnold, P. L.; McMullon, M. W.; Rieb, J.; Kühn, F. E., *Angew. Chem., Int. Ed. Engl.* **2015,** *54* (1), 82-100.
2. Evans, W. J.; Champagne, T. M.; Ziller, J. W., *J. Am. Chem. Soc.* **2006,** *128* (44), 14270-14271.
3. Evans, W. J.; Miller, K. A.; DiPasquale, A. G.; Rheingold, A. L.; Stewart, T. J.; Bau, R., *Angew. Chem., Int. Ed. Engl.* **2008,** *47* (27), 5075-5078.
4. Higgins, J. A.; Cloke, F. G. N.; Roe, S. M., *Organometallics* **2013,** *32* (19), 5244-5252.
5. Evans, W. J.; Davis, B. L.; Champagne, T. M.; Ziller, J. W., *Proc. Natl. Acad. Sci.* **2006,** *103* (34), 12678-12683.
6. Scott, J.; Basuli, F.; Fout, A. R.; Huffman, J. C.; Mindiola, D. J., *Angew. Chem., Int. Ed. Engl.* **2008,** *47* (44), 8502-8505.
7. Jian, Z.; Rong, W.; Mou, Z.; Pan, Y.; Xie, H.; Cui, D., *Chem. Commun.* **2012,** *48* (60), 7516-7518.
8. King, D. M.; Tuna, F.; McInnes, E. J. L.; McMaster, J.; Lewis, W.; Blake, A. J.; Liddle, S. T., *Science* **2012,** *337* (6095), 717-720.
9. King, D. M.; Tuna, F.; McInnes, E. J. L.; McMaster, J.; Lewis, W.; Blake, A. J.; Liddle, S. T., *Nat Chem* **2013,** *5* (6), 482-488.

10. Straub, T.; Haskel, A.; Neyroud, T. G.; Kapon, M.; Botoshansky, M.; Eisen, M. S., *Organometallics* **2001,** *20* (24), 5017-5035.
11. Goldman, A. S.; Goldberg, K. I., Preface. In *Activation and Functionalization of C-H Bonds*, American Chemical Society: 2004; Vol. 885.
12. Arockiam, P. B.; Bruneau, C.; Dixneuf, P. H., *Chem. Rev.* **2012,** *112* (11), 5879-5918.
13. Reynolds, L. T.; Wilkinson, G., *J. Inorg. Nucl. Chem.* **1956,** *2*, 246-53.
14. Thomson, R. K.; Cantat, T.; Scott, B. L.; Morris, D. E.; Batista, E. R.; Kiplinger, J. L., *Nat Chem* **2010,** *2* (9), 723-729.
15. Fox, A. R.; Bart, S. C.; Meyer, K.; Cummins, C. C., *Nature* **2008,** *455* (7211), 341-349.
16. Pool, J. A.; Scott, B. L.; Kiplinger, J. L., *J. Am. Chem. Soc.* **2005,** *127* (5), 1338-1339.
17. Manriquez, J. M.; Fagan, P. J.; Marks, T. J., *J. Am. Chem. Soc.* **1978,** *100* (12), 3939-3941.
18. Evans, W. J.; Walensky, J. R.; Ziller, J. W.; Rheingold, A. L., *Organometallics* **2009,** *28* (12), 3350-3357.
19. Andrea, T.; Barnea, E.; Eisen, M. S., *J. Am. Chem. Soc.* **2008,** *130* (8), 2454-2455.
20. Jantunen, K. C.; Burns, C. J.; Castro-Rodriguez, I.; Da Re, R. E.; Golden, J. T.; Morris, D. E.; Scott, B. L.; Taw, F. L.; Kiplinger, J. L., *Organometallics* **2004,** *23* (20), 4682-4692.
21. Fagan, P. J.; Manriquez, J. M.; Maatta, E. A.; Seyam, A. M.; Marks, T. J., *J. Am. Chem. Soc.* **1981,** *103* (22), 6650-6667.
22. Jia, L.; Yang, X.; Stern, C. L.; Marks, T. J., *Organometallics* **1997,** *16* (5), 842-857.
23. Haskel, A.; Straub, T.; Eisen, M. S., *Organometallics* **1996,** *15* (18), 3773-3775.
24. Chen, Y.-X.; Metz, M. V.; Li, L.; Stern, C. L.; Marks, T. J., *J. Am. Chem. Soc.* **1998,** *120* (25), 6287-6305.
25. Bruno, J. W.; Marks, T. J.; Morss, L. R., *J. Am. Chem. Soc.* **1983,** *105* (23), 6824-6832.
26. Pagano, J. K.; Dorhout, J. M.; Czerwinski, K. R.; Morris, D. E.; Scott, B. L.; Waterman, R.; Kiplinger, J. L., *Organometallics* **2016,** *35* (5), 617-620.
27. Siladke, N. A.; Webster, C. L.; Walensky, J. R.; Takase, M. K.; Ziller, J. W.; Grant, D. J.; Gagliardi, L.; Evans, W. J., *Organometallics* **2013,** *32* (21), 6522-6531.
28. Langeslay, R. R.; Fieser, M. E.; Ziller, J. W.; Furche, F.; Evans, W. J., *J. Am. Chem. Soc.* **2016,** *138* (12), 4036-4045.
29. Arnold, P. L.; Farnaby, J. H.; White, R. C.; Kaltsoyannis, N.; Gardiner, M. G.; Love, J. B., *Chem. Sci.* **2014,** *5* (2), 756-765.
30. Lin, Z.; Le Marechal, J. F.; Sabat, M.; Marks, T. J., *J. Am. Chem. Soc.* **1987,** *109* (13), 4127-4129.
31. Yang, X.; King, W. A.; Sabat, M.; Marks, T. J., *Organometallics* **1993,** *12* (10), 4254-4258.
32. Ren, W.; Zi, G.; Fang, D.-C.; Walter, M. D., *Chem. Eur. J.* **2011,** *17* (45), 12669-12682.
33. Langeslay, R. R.; Walensky, J. R.; Ziller, J. W.; Evans, W. J., *Inorg. Chem.* **2014,** *53* (16), 8455-8463.
34. Yang, X.; Stern, C.; Marks, T. J., *Organometallics* **1991,** *10* (4), 840-842.
35. Trnka, T. M.; Bonanno, J. B.; Bridgewater, B. M.; Parkin, G., *Organometallics* **2001,** *20* (15), 3255-3264.
36. Hall, S. W.; Huffman, J. C.; Miller, M. M.; Avens, L. R.; Burns, C. J.; Sattelberger, A. P.; Arney, D. S. J.; England, A. F., *Organometallics* **1993,** *12* (3), 752-758.
37. Mora, E.; Maria, L.; Biswas, B.; Camp, C.; Santos, I. C.; Pécaut, J.; Cruz, A.; Carretas, J. M.; Marçalo, J.; Mazzanti, M., *Organometallics* **2012,** *32* (5), 1409-1422.
38. Hayes, C. E.; Platel, R. H.; Schafer, L. L.; Leznoff, D. B., *Organometallics* **2012,** *31* (19), 6732-6740.
39. Cruz, C. A.; Emslie, D. J. H.; Robertson, C. M.; Harrington, L. E.; Jenkins, H. A.; Britten, J. F., *Organometallics* **2009,** *28* (6), 1891-1899.
40. Fendrick, C. M.; Schertz, L. D.; Day, V. W.; Marks, T. J., *Organometallics* **1988,** *7* (8), 1828-1838.
41. Fendrick, C. M.; Mintz, E. A.; Schertz, L. D.; Marks, T. J., *Organometallics* **1984,** *3* (5), 819-821.
42. Edwards, P. G.; Andersen, R. A.; Zalkin, A., *Organometallics* **1984,** *3* (2), 293-298.
43. Cruz, C. A.; Emslie, D. J. H.; Harrington, L. E.; Britten, J. F., *Organometallics* **2008,** *27* (1), 15-17.
44. Button, Z. E.; Higgins, J. A.; Suvova, M.; Cloke, F. G. N.; Roe, M., *Dalton Trans.* **2015,** *44* (6), 2588-2596.
45. Ren, W.; Zhao, N.; Chen, L.; Zi, G., *Inorg. Chem. Commun.* **2013,** *30*, 26-28.
46. Fortier, S.; Melot, B. C.; Wu, G.; Hayton, T. W., *J. Am. Chem. Soc.* **2009,** *131* (42), 15512-15521.
47. Jantunen, K. C.; Haftbaradaran, F.; Katz, M. J.; Batchelor, R. J.; Schatte, G.; Leznoff, D. B., *Dalton Trans.* **2005,** *0* (18), 3083-3091.
48. Cordero, B.; Gomez, V.; Platero-Prats, A. E.; Reves, M.; Echeverria, J.; Cremades, E.; Barragan, F.; Alvarez, S., *Dalton Trans.* **2008,** (21), 2832-2838.
49. Dash, A. K.; Wang, J. Q.; Wang, J.; Gourevich, I.; Eisen, M. S., *J. Nucl. Sci. Technol.* **2002,** *39* (sup3), 386-392.
50. Dash, A. K.; Wang, J. Q.; Eisen, M. S., *Organometallics* **1999,** *18* (23), 4724-4741.
51. Haskel, A.; Straub, T.; Dash, A. K.; Eisen, M. S., *J. Am. Chem. Soc.* **1999,** *121* (13), 3014-3024.
52. Thomson, R. K.; Graves, C. R.; Scott, B. L.; Kiplinger, J. L., *Eur. J. Inorg. Chem.* **2009,** *2009* (11), 1451-1455.
53. Evans, W. J.; Siladke, N. A.; Ziller, J. W., *C. R. Chim.* **2010,** *13* (6-7), 775-780.
54. Montalvo, E.; Ziller, J. W.; DiPasquale, A. G.; Rheingold, A. L.; Evans, W. J., *Organometallics* **2010,** *29* (9), 2104-2110.
55. Evans, W. J.; Walensky, J. R.; Ziller, J. W., *Organometallics* **2010,** *29* (4), 945-950.
56. Graves, C. R.; Scott, B. L.; Morris, D. E.; Kiplinger, J. L., *Organometallics* **2008,** *27* (14), 3335-3337.
57. Newell, B. S.; Rappé, A. K.; Shores, M. P., *Inorg. Chem.* **2010,** *49* (4), 1595-1606.
58. R. Crampton, M.; A. Robotham, I., *J. Chem. Res., Synop.* **1997,** (1), 22-23.
59. Cruz, C. A.; Emslie, D. J. H.; Harrington, L. E.; Britten, J. F., *Organometallics* **2007,** *27* (1), 15-17.
60. Korobkov, I.; Vidjayacoumar, B.; Gorelsky, S. I.; Billone, P.; Gambarotta, S., *Organometallics* **2010,** *29* (3), 692-702.
61. Korobkov, I.; Gambarotta, S.; Yap, G. P. A., *Angew. Chem., Int. Ed. Engl.* **2003,** *42* (7), 814-818.
62. McKinven, J.; Nichol, G. S.; Arnold, P. L., *Dalton Trans.* **2014,** *43* (46), 17416-17421.
63. Arnold, P. L.; Farnaby, J. H.; Gardiner, M. G.; Love, J. B., *Organomet.* **2015,** *34* (11), 2114-2117.
64. Dutkiewicz, M. S.; Farnaby, J. H.; Apostolidis, C.; Colineau, E.; Walter, O.; Magnani, N.; Gardiner, M. G.; Love, J. B.; Kaltsoyannis, N.; Caciuffo, R.; Arnold, P. L., *Nat Chem* **2016,** *8* (8), 797-802.
65. Arnold, P. L.; Stevens, C. J.; Farnaby, J. H.; Gardiner, M. G.; Nichol, G. S.; Love, J. B., *J. Am. Chem. Soc.* **2014,** *136* (29), 10218-10221.
66. Gilbert, T. M.; Ryan, R. R.; Sattelberger, A. P., *Organometallics* **1988,** *7* (12), 2514-2518.
67. Stubbert, B. D.; Marks, T. J., *J. Am. Chem. Soc.* **2007,** *129* (19), 6149-6167.
68. Butcher, R. J.; Clark, D. L.; Grumbine, S. K.; Watkin, J. G., *Organometallics* **1995,** *14* (6), 2799-2805.
69. Turner, H. W.; Andersen, R. A.; Zalkin, A.; Templeton, D. H., *Inorg. Chem.* **1979,** *18* (5), 1221-1224.
70. Ilango, S.; Vidjayacoumar, B.; Gambarotta, S., *Dalton Trans.* **2010,** *39* (29), 6853-6857.

71. Bettonville; S.; Goffart; J.; Fuger; J., *Organo-f-element thermochemistry. Actinide-ligand bond disruption enthalpies in tris(indenyl)actinide hydrocarbyls*. Elsevier: Lausanne, SUISSE, 1989; Vol. 377.
72. Bruno, J. W.; Stecher, H. A.; Morss, L. R.; Sonnenberger, D. C.; Marks, T. J., *J. Am. Chem. Soc.* **1986,** *108* (23), 7275-7280.
73. Schock, L. E.; Seyam, A. M.; Sabat, M.; Marks, T. J., *Polyhedron* **1988,** *7* (16–17), 1517-1529.
74. Bordwell, F. G., *Acc. Chem. Res.* **1988,** *21* (12), 456-463.
75. Arnold, P. L.; Turner, Z. R., *Nat. Rev. Chem.* **2017,** *1*, 0002.
76. Matson, E. M.; Fanwick, P. E.; Bart, S. C., *Organometallics* **2011,** *30* (21), 5753-5762.
77. Rosenthal, U.; Pulst, S.; Arndt, P.; Ohff, A.; Tillack, A.; Baumann, W.; Kempe, R.; Burlakov, V. V., *Organometallics* **1995,** *14* (6), 2961-2968.
78. Shang-Chao, D.; Hua-Qiao, T.; Yan-Feng, B.; Yang, Y.; Wu-Ping, L., *Chin. J. Inorg. Chem.* **2014,** *30* (4), 749-756.
79. Ritchey, J. M.; Zozulin, A. J.; Wrobleski, D. A.; Ryan, R. R.; Wasserman, H. J.; Moody, D. C.; Paine, R. T., *J. Am. Chem. Soc.* **1985,** *107* (2), 501-503.
80. Bond, A. D.; Davies, J. E., *Acta Crystallogr., Sect. E* **2002,** *58* (7), o777-o778.
81. Bailey, P. J.; Coxall, R. A.; Dick, C. M.; Fabre, S.; Henderson, L. C.; Herber, C.; Liddle, S. T.; Loroño-González, D.; Parkin, A.; Parsons, S., *Chem. Eur. J.* **2003,** *9* (19), 4820-4828.
82. Assadi, M. G.; Mahkam, M.; Tajrezaiy, Z., *Heteroat. Chem.* **2007,** *18* (4), 414-420.
83. Mansell, S. M.; Perandones, B. F.; Arnold, P. L., *J. Organomet. Chem. 695* (25–26), 2814-2821.
84. Cantat, T.; Scott, B. L.; Kiplinger, J. L., *Chem. Commun.* **2010,** *46* (6), 919-921.
85. Sessler, J. L.; Cho, W.-S.; Lynch, V.; Kral, V., *Chem. - Eur. J.* **2002,** *8* (5), 1134-1143.
86. Hitchcock, P. B.; Khvostov, A. V.; Lappert, M. F., *J. Organomet. Chem.* **2002,** *663* (1-2), 263-268.
87. Sheldrick, G., *Acta Crystallogr., Sect. A:* **2015,** *71* (1), 3-8.
88. Dolomanov, O. V.; Bourhis, L. J.; Gildea, R. J.; Howard, J. A. K.; Puschmann, H., *J. Appl. Crystallogr.* **2009,** *42* (2), 339-341.
89. M. J. Frisch, G. W. T., H. B. Schlegel, G. E. Scuseria, M. A. Robb, J. R. Cheeseman, G. Scalmani, V. Barone, B. Mennucci, G. A. Petersson, H. Nakatsuji, M. Caricato, X. Li, H. P. Hratchian, A. F. Izmaylov, J. Bloino, G. Zheng, J. L. Sonnenberg, M. Hada, M. Ehara, K. Toyota, R. Fukuda, J. Hasegawa, M. Ishida, T. Nakajima, Y. Honda, O. Kitao, H. Nakai, T. Vreven, J. A. Montgomery, Jr., J. E. Peralta, F. Ogliaro, M. Bearpark, J. J. Heyd, E. Brothers, K. N. Kudin, V. N. Staroverov, R. Kobayashi, J. Normand, K. Raghavachari, A. Rendell, J. C. Burant, S. S. Iyengar, J. Tomasi, M. Cossi, N. Rega, J. M. Millam, M. Klene, J. E. Knox, J. B. Cross, V. Bakken, C. Adamo, J. Jaramillo, R. Gomperts, R. E. Stratmann, O. Yazyev, A. J. Austin, R. Cammi, C. Pomelli, J. W. Ochterski, R. L. Martin, K. Morokuma, V. G. Zakrzewski, G. A. Voth, P. Salvador, J. J. Dannenberg, S. Dapprich, A. D. Daniels, Ö. Farkas, J. B. Foresman, J. V. Ortiz, J. Cioslowski, and D. J. Fox, Gaussian 09, Revision D.01. Gaussian, Inc.: Wallingford CT, 2009.
90. Barone, C. A. a. V., *J. Chem. Phys.* **1999,** *110*, 6158.
91. Jr., T. H. D., *J. Chem. Phys.* **1989,** *90*, 1007.
92. R. A. Kendall, T. H. D. J., and R. J. Harrison, *J. Chem. Phys.* **1992,** *96*, 6796.
93. W. Küchle, M. D., H. Stoll and H. Preuss, *J. Chem. Phys.* **1994,** *100*, 7535.
94. X. Cao, M. D. a. H. S., *J. Chem. Phys.* **2003,** *118*, 487.
95. M. Dolg, U. W., H. Stoll and H. Preuss, *J. Chem. Phys.* **1987,** *86*, 866.
96. Sundermann, J. M. L. M. a. A., *J. Chem. Phys.* **2001,** *114*, 3408.
97. D. Figgen, K. A. P., M. Dolg and H. Stoll, *J. Chem. Phys.* **2009,** *130*, 164108.
98. Tomasi, J.; Mennucci, B.; Cammi, R., *Chem. Rev.* **2005,** *105* (8), 2999-3094.
99. Cancès, E.; Mennucci, B.; Tomasi, J., *The Journal of Chemical Physics* **1997,** *107* (8), 3032-3041.
100. Cossi, M.; Barone, V.; Cammi, R.; Tomasi, J., *Chem. Phys. Lett.* **1996,** *255* (4), 327-335.
101. Miertuš, S.; Tomasi, J., *Chem. Phys.* **1982,** *65* (2), 239-245.
102. Miertuš, S.; Scrocco, E.; Tomasi, J., *Chem. Phys.* **1981,** *55* (1), 117-129.
103. Pascual-ahuir, J. L.; Silla, E.; Tuñon, I., *J. Comput. Chem.* **1994,** *15* (10), 1127-1138.

Table of Contents artwork